Functional interaction between TRPM2 and $IK_{ca}1$ ion channels in mouse microglia

Deveci, Aykut

Doctor of Philosophy

Department of Physiological Sciences,

School of Life Science,

The Graduate University for Advanced Studies, SOKENDAI

2022

Summary

TRPM2 is a nonselective, calcium (Ca^{2+})-permeable cation channel and is expressed in various organs such as the brain, pancreas, spleen, kidney and a wide range of immunocytes, including lymphocytes, neutrophils and monocytes/macrophages. TRPM2 plays important roles in Ca^{2+} signaling in these tissues and cells, and contributes to cellular functions that include insulin release, cytokine production, cell motility and cell death. The primary activator of TRPM2 is adenosine diphosphate ribose (ADPR) and the activation induces a Ca^{2+} influx into the interior of the cells.

The Ca^{2+} influx induced by TRPM2 may activate other Ca^{2+}-dependent channels. The intermediate conductance Ca^{2+}-activated potassium channel ($IK_{Ca}1$ / KCa3.1 / SK4) is of particular interest. The Ca^{2+} affinity for the $IK_{Ca}1$ channel is provided by calmodulin (CaM) via lobes present on the protein. Once CaM is activated by Ca^{2+} binding, the $IK_{Ca}1$ channel is opened, allowing potassium (K^+) efflux from the intracellular compartment to the extracellular medium. K^+ movement is accompanied by chloride (Cl^-) efflux and water loss that promotes different physiological processes such as proliferation, migration, cell volume changes, cytokine production and inflammation.

To initiate this study, I used HEK293T cells in order to assess if TRPM2 and $IK_{Ca}1$ channels collaborated. I used different pharmacological tools as ADPR and TRAM-34 (a specific inhibitor of $IK_{Ca}1$ channels) to discriminate between the channels. After confirming that these channels constituted a network and confirming their physical interaction by examining the E_{rev} value shift, I noticed that they cause cell volume changes. Based on those results, I extended the experiments to mouse primary microglia because both of the channels are expressed in this cell. The literature confirmed that microglia express both TRPM2 and $IK_{Ca}1$ channels. After assessing the purity of the microglia that I isolated from new-born (days 1 – 3) mice, I demonstrated that the TRPM2 /

$IK_{Ca}1$ channel network functioned in mouse primary microglia based on the E_{rev} value shift. I demonstrated that this network could also take part in cell volume changes in mouse primary microglia. Based upon that information, I hypothesized that cell volume changes could be linked to cell migration. In that regard, understanding how microglia proliferate and migrate could suggest improved strategies for treatments of CNS-linked diseases.

It is known that microglia adopt different states in response to the changes in their microenvironment, i.e., an active state and a resting state. The different states of microglia could be associated with the intensity and duration of the pathological environment. When microglia are subjected to homeostatic disturbances, for example neuroinflammation or injury, these cells become activated. The activated state is phenotypically characterized by the retraction of ramifications, swelling of the soma, and an overall amoeboid appearance. This phenotype confers motility to microglia and allows them to move by following the chemotactic gradient towards the site of injury. Migration of microglia can be described as a repeated and coordinated cycle of protrusion of the front and retraction of the tail portion. Here, I demonstrated that cell volume changes are correlated with microglial migration, meaning that the TRPM2 / $IK_{Ca}1$ network is implicated in the motility of mouse primary microglia. I describe for the first time that inhibiting the $IK_{Ca}1$ channel decreases the motility of mouse primary microglia *in vitro*.

Next, I investigated whether the TRPM2 / $IK_{Ca}1$ network was implicated in cytokine production. Microglia are mainly involved in CNS homeostasis by monitoring changes in their microenvironment (resting state) or by adopting protective features, such as initiating their own inflammatory response (activated state). I found that the TRPM2 / $IK_{Ca}1$ network was essential for IL-1β production. Taken together, these results deepen our understanding of microglia phenotypes and function.

This novel TRPM2 / $IK_{Ca}1$ ion channel network might provide new approaches to neurologic and physiological research and lead to new tools for the prevention or cure of CNS-linked diseases.

Index

1. Introduction

The divalent cation calcium (Ca^{2+}) is an important element in the human body as it plays essential physiological roles. Intracellular free cytosolic Ca^{2+} concentrations are maintained at around 100 nM whereas the extracellular milieu contains roughly 1 mM Ca^{2+} (Rizzuto, R. and Pozzan, T., 2006; Raffaello, A. et al., 2016; Yang, Z. et al., 2015). Within cells, the maintenance of Ca^{2+} at a nM concentration requires specific proteins that contain sites with particular affinities and specificities like calmodulin (CAM), STIM1 (stromal interaction molecule-1), S100 proteins, C_2 domain and the Annexin Ca^{2+}-binding fold. These proteins sequester Ca^{2+} inside cellular organelles, including the endoplasmic reticulum (ER), Golgi apparatus (Raffaello, A. et al., 2016; Yang, Z. et al., 2015) or organized in insoluble non-membranous structures such as the cytoskeleton. They buffer Ca^{2+} within a nM range without modifying its total content in the cells (Carafoli, E. and Krebs, J. 2016). Ca^{2+} is used by cells to monitor and control many of their activities. Once specialized functions are acquired by cells, Ca^{2+} is used as an intracellular signalling messenger that controls many diverse processes like proliferation, contraction and excitation in a range of cell types (Pinto, M.C.X. et al., 2015; Munaron, L. et al., 2004; Clapham, D.E., 2007). It is also involved in the physiopathology of the cells and cell fate. Moreover, Ca^{2+} is one of the most-common and important ions in eukaryotic cells. The homeostasis of Ca^{2+} is crucial for cell survival (Mincheva-Tasheva, S. et al., 2014). To maintain this homeostasis, ion exchanges between cells or the extracellular compartment occur (Brini, M. et al., 2013; Clapham, D.E., 2007). The fluxes of Ca^{2+} are mediated by transporters located on the plasma membrane and the membrane of intracellular compartments that are permeable to Ca^{2+} (Islam, M.S., 2020). The transporters are termed ion channels, and they are pore forming proteins docked on the cell membranes. Ion channels are distributed in all the tissues of an organism. Among these channels, it was reported in numerous studies that transient receptor potential (TRP) channels serve as

biosensors by mediating responses to variations in different environmental conditions (Nilius, B. et al., 2007; Kaneko, Y. et al., 2014). There are 28 mammalians (27 human) TRP channels that have been described as polymodal cell sensors (Nilius, B. and Owsianik, G., 2011) and they play important roles in many homeostatic functions. They are separated into six subfamilies: TRPC (canonical 1-7), TRPV (vanilloid 1-6), TRPP (polycystin (TRPP 2-3-5), TRPML (mucolipin 1-8), TRPA (ankyrin 1) and TRPM (melastatin 1-8). In the TRP channel family, TRP Melastatin 2 (TRPM2) is highly expressed in the brain and is also detected in other tissues such as lung, liver, bone marrow, spleen and heart. At the cellular level, TRPM2 has been identified in multiple cell types like neurons (Bai, J. Z. and Lipski, J, 2010; Alim, I. et al., 2013), microglia (Fonfria, E. et al., 2006; Jeong, H. et al., 2017), astrocytes (Lee, M. et al., 2010), macrophages (Di, A. et al., 2017, Kashio, M. et al., 2012), neutrophils (Heiner et al., 2003), dendritic cells (Sumoza-Toledo, A. et al., 2011), endothelial vascular cells (Hecquet, C. M. et al., 2010) and pancreatic β-cells (Ishii, M. et al., 2006; Togashi, K. et al., 2008). The *TRPM2* gene is localized in the q22.31 locus on human chromosome 21. It is a Ca^{2+}-permeable, non-selective cation channel that exhibits heat sensitivity. It acts as a biosensor of oxidative and osmotic stresses under physiological and pathological conditions. In addition to its role as a plasma membrane channel, TRPM2 has been shown to be localized to the lysosomal compartment, where it regulates Ca^{2+} mobilization from the intracellular compartments and contributes to H_2O_2-induced apoptosis of β cells (Turlova, E. et al., 2018). The abundant distribution of TRPM2 indicates that it may play roles in a wide range of physiological processes, including synaptic transmission in hippocampal CA3-CA1 synapses where TRPM2 is activated following Ca^{2+} increases mediated by voltage-dependent Ca^{2+} channels and glutamate receptors (Olah, M. E. et al., 2009). Additional roles for TRPM2 in the central nervous system (CNS) are related to its presence in microglia, the host macrophages of the brain, where TRPM2 appears to be responsible for physiological microglial activation through reactive oxygen species (ROS) and lipopolysaccharide (LPS)-mediated signalling (Kraft, R. et al., 2004). However, the majority of

studies place TRPM2 into the context of pathophysiological events of stroke/ischemia and neurodegeneration (Xie, Y. F. et al., 2011), where TRPM2 activation results in the promotion of cytokine release, the exacerbation of inflammation, and the initiation of neuronal death.

In terms of structure, TRPM2 is a homotetrameric protein, meaning that it is formed by 4 identical subunits. Each of these subunits is made of 1503 amino acid residues (Szollosi, A., 2021) with a molecular mass around 170 kDa. Each subunit is divided into 3 regions: a large cytosolic N-terminus, followed by a transmembrane domain region (TMD) and finally a cytosolic C-terminus. If we focus on each of these regions, each of them has a ligand binding domain involved in TRPM2 activation. TMD includes approximately 400 amino acids (from 650 to 1050 amino acids (Figure 1)) (Cheung, J. A. et al., 2017) that form 6 transmembrane helices (S1 - S6) throughout the plasma membrane, in which the S5-S6 region constitutes a pore domain allowing permeation of ions once the channel is activated. To activate this channel, a different ligand needs to bind to the specific site. TRPM2 requires intracellular Ca^{2+} binding (Penner. R, 2007) and two Adenosine Diphosphate Ribose (ADPR) binding stimuli in cytosolic N-terminal and C-terminal regions to be activated.

ADPR is a nicotinamide adenine dinucleotide (NAD^+)-derived metabolite. ADPR can be produced by several metabolic pathways. Under oxidative stress conditions, reactive oxygen species (ROS) produce poly-ADPR polymerase (PARP) and poly-ADPR glycohydrolase (PARG), which are DNA repair enzymes. Thereafter, PARP-1 (the most abundant of the PARP family) catalyzes NAD^+ into nicotinamide and ADPR, and polymerises ADPR onto various nuclear proteins including poly-ADPR (Soldani, C. et al., 2002; Fonfria, E. et al., 2004). The poly-ADPR molecule is then hydrolysed by PARG for ADPR production (Kolisek, M. et al., 2005). ADPR and its precursor might also be released from mitochondrial permeability transition pores located on the mitochondrial matrix.

The N- and C-termini of TRPM2 accept ADPR. The N-terminus consists of 4 TRPM subfamily homologous domains (MHD I-IV) and a CaM-binding IQ-like motif located between MHDII

and MHDIII (Figure 1). The main stimulus that triggers TRPM2 activation is ADPR binding in the cleft of the MHDI/II domain. Indeed, ADPR is inserted between tyrosine 295 (Y295) and the loop connecting the β5 strand α3 helix (β5-α3 loop) with a compact U shape in order to adapt to the bi-lobed structure of the MHDI/II domain that is deep, small and circular (Figure 2 B, C) (Huang, Y. et al., 2019). ADPR is kept in this cleft by interacting with its different groups.

The C-terminus is constituted by a TRP Box domain (hydrophobic and highly conserved region among TRPs channels) that is located downstream from the pore region. The coiled-coil motif is essential for the assembly of homomeric and heteromeric protein complexes and protein-protein interaction, including TRPM2 subunit interaction that is required for a functional channel. Finally, there is a nucleoside diphosphate-linked moiety X-type motif 9 domain (NUDT9-H). ADPR binds to NUDT9-H. This domain is composed of around a 50 amino acid Nudix box motif (which is an ADPR pyrophosphatase (ADPRase)) and cleaved into adenosine monophosphate (AMP) and ribose-5-phosphate). It is defined as a catalytic site found within a larger domain of roughly 300 amino acids. (Figure 1). In contrast to the cleft of MHDI/II domain, the NUDT9-H cleft is larger and allows ADPR to be linked with an extended shape (Figure 2 D-E) (Huang, Y. et al., 2019).

When all of the ligands are bound to their specific binding sites, a rotation of the subunit occurs. The resting gate that displays a radius of 1.0 Å and prevents permeation is then enlarged to 2.6 Å in the TMD region, allowing the passage of Ca^{2+} and Na^{+} ions from the extracellular compartment towards the intracellular compartment (Huang, Y. et al., 2018).

The Ca^{2+} influx induced by TRPM2 may activate other Ca^{2+}-dependent channels.

Ca^{2+}-activated potassium channels constitute a heterogeneous family of ion channels with variable biophysical and pharmacological properties. Among them, the intermediate conductance calcium-activated potassium channel ($IK_{Ca}1$/ KCa3.1/ SK4) is of interest. This channel is encoded by the *KCNN4* gene located in the q13.2 locus of human chromosome 19. These

channels share a common functional role by coupling the increase in intracellular Ca^{2+} concentration to hyperpolarization of the membrane potential. The activity of the $IK_{Ca}1$ channel is independent of the membrane potential (Suppiramaniam, V. et al., 2010). This intrinsic feature allows the $IK_{Ca}1$ channel to play key roles in controlling cellular excitability and maintaining K^+ homeostasis and cell volume in non-excitable cells (Kshatri, A. S. et al., 2018). $IK_{Ca}1$ channels are responsible for activation and proliferation of smooth muscle cells and lymphocytes (Toyama, K. et al., 2008). In the CNS, $IK_{Ca}1$ channels are mainly localized in microglia and endothelial cells (Pedarzani, P. and Stocker M., 2008). Microglial $IK_{Ca}1$ channels participate in controlling several functions, including respiratory burst, proliferation, migration as well as LPS-mediated nitric oxide production (Nguyen, H. M. et al., 2017). Accumulating evidence indicates that $IK_{Ca}1$ channels are involved in the process of astrogliosis, which occurs in most forms of CNS insult (Bouhy, D. et al., 2011). $IK_{Ca}1$ channels also contribute to neurovascular coupling in astrocytes (Longden, T. A. et al., 2011).

In terms of structure, the functional $IK_{Ca}1$ channel is a homotetramer formed by four identical subunits each carrying a CaM molecule. Each channel subunit is made of 427 amino acids (predicted molecular mass around 48 kDa) that constitute the six TMD (S1 - S6) and cytosolic N and C termini (Weisbrod, D., 2020; Ledoux, J. et al., 2006). Between S5 (amino acid 203) and S6 (amino acid 287), a hydrophobic segment forms the pore motif (P-Loop) and this pore has a "selectivity filter" for potassium (K^+) given by the GYG consensus motif (Figure 3).

Between the segment composed of amino acids 312-329, located on the C-terminal, HA and HB helix cross one another. The intertwining of these helices creates the calmodulin binding domain CamBD1. Parallel to the membrane, this region is pre-associated with the C-lobe of CaM (there is also an N-lobe) in a Ca^{2+}-independent manner. Ca^{2+} sensitivity is conferred to the $IK_{Ca}1$ channel by CaM. CaM is composed of 148 amino acids (around 17 kDa). C- and N- lobes possess two pairs of helix-loop-helix (EF-hand) each that enable the binding of four Ca^{2+} ions on the sites. A long and highly flexible α helix, connecting the lobes, allows the protein to adopt

different conformations with varying affinities to target Ca^{2+} binding. At low intracellular Ca^{2+} threshold concentrations, the N-lobes are close to the S2-S3 intracellular segment. The N iii binding site (located on the N lobe) particularly shows higher affinity to Ca^{2+}. Indeed, after Ca^{2+} binds to site iii of CaM, this interaction triggers a conformational change of the molecule that increases its affinity for Ca^{2+} binding to the three other available sites (Catacuzenno, L. et al., 2018). It is also well known that CaM binds strongly and in a Ca^{2+}-independent manner to the first 62 amino acids of $IK_{Ca}1$'s C-terminus (Figure 3).

The segment corresponding to the HC helix forms CamBD2 and is located between amino acids 360-373 (Figure 3). Pointed towards the cytosol, it is associated with similar helices from the other subunits' coiled-coil structure and is essential for the proper assembly and trafficking of the channel by protein kinase A (PKA), AMP-activated protein kinase (AMPK) and phosphatidylinositol 3-phosphate (PI3P). Once CaM is activated by Ca^{2+} binding, N lobes recognize the CamBD2 segment of the closest subunit of the homotetramer. This interaction pulls the C-terminal of the subunits and opens the $IK_{Ca}1$ channel, which allows K^+ efflux from the intracellular compartment towards the extracellular compartment of the cell. The intracellular change in K^+ concentration promotes several intracellular signalling pathways that are involved in different physiological processes such as proliferation, migration, cell volume changes, inflammation and apoptosis. (Schwab, A. et al., 2012; Hayabuchi, Y., 2017; Takayama, Y. 2014; Nguyen, H.M, 2017).

Microglia cells were discovered by Rio-Hortega. (Kettenmann, H. et al., 2011). They can proliferate, migrate and produce cytokines. These non-excitable cells, expressing both TRPM2 and $IK_{Ca}1$ channels (Brown, B. M. et al., 2018 and 2019; Sita, G. et al., 2018; Bouhy, D. et al., 2011), are described as a specialized population of primary innate immune cells in the CNS (Marin-Teva, J. L. et al., 2011). The microglia population represents 0.5-16.6% of the total cell population in the human brain and 5-12% in the mouse brain. These cells originate from yolk sac

progenitors and they are widely considered to be equivalent throughout the CNS (De Biase, L. M. et al., 2017). They are mainly involved in CNS homeostasis by monitoring changes in their microenvironment (resting state) or by adopting protective features, such as initiating their own inflammatory response in order to modulate these changes (activated state) (Nimmerjahn, A. et al., 2005; Wolf, S. A. et al., 2017). In the resting state, microglia are characterized by a ramified morphology: a small soma with fine cellular processes that are able to sense damage signals within the surrounding microenvironment. When microglia are subjected to homeostatic disturbances, for example neuroinflammation or after injury, these cells become activated. This activated state is phenotypically characterized by the retraction of its ramifications, swelling of the soma, and an overall amoeboid appearance. This phenotype confers motility to microglia and allows them to move actively by following the chemotactic gradient towards the injured site. Migration of microglia can be described as a repeated and coordinated cycle of protrusion of the front and retraction of the tail part. Protrusion of the front and retraction of the tail parts of microglia requires that the respective components of the cellular migrating machinery, e.g., polymerizing actin filaments at the cell front and contractile protein at the tail part, are differentially localized and regulated within the microglia (Schwab, A. et al., 2012). Microglial activity is involved in the development, maturation and senescence of the CNS throughout life by taking part in the development of synaptic growth and plasticity, and in neuronal apoptosis. Indeed, a decrease in branches of microglia is observed in ageing brains. This induces a reduction of surveillance area. Early publications (decades ago) established that microglial cells play an essential role in the aging brain and various CNS-related diseases, including ischemic stroke, traumatic brain damage, Alzheimer's disease (AD), Parkinson's disease (PD), multiple sclerosis (MS) and amyotrophic lateral sclerosis (ALS). In each case, microglial cells mediate neuroinflammation. Indeed, the unphysiological activation of microglia contributes to neurotoxicity and synapse loss by triggering several proinflammatory cascades that lead to neuron-microglia network impairment (Sarlus, H. and Heneka, M. T., 2017). These different

states of microglia could be associated with the intensity and duration of the pathological environment. Dysregulation of neuron-microglia communication is likely a primary pathologic event in neurodegenerative diseases.

2. Materials and Methods

2.1. Animals

57BL/6NCr mice (SLC Japan) were used as the WT strain. TRPM2 KO mice were generously provided by Dr. Yasuo Mori (Kyoto University, Japan) (53). For *in vitro* time-lapse imaging, postnatal pups (P0 through P3) were obtained from TRPM2KO genotype mice. Mice were housed in a controlled environment (12 h light/12 h dark cycle; room temperature, 22°C to 24°C; 50 to 60% relative humidity) with free access to food and water. All procedures involving the care and use of animals were approved by the Institutional Animal Care and Use Committee of the National Institutes of Natural Sciences and carried out in accordance with the NIH Guide for the care and use of laboratory animals (NIH publication no. 85–23, revised 1985).

2.2. Preparation of Primary Mouse Microglia

Primary mouse microglia were obtained according to a previously described method (Doering, L. C., 2010) with modification. Mixed glial cultures were prepared from cerebral hemispheres of postnatal (P0 through P3) pups. The tissues were minced with a sterile Pasteur pipette (IWAKI) and trypsinized (Gibco) for 8 min at 37°C. Then, DNase (Roche, 11056000) was added and the suspension was immediately mixed. After that, one volume of horse serum (Biowest, S0900) was added and again the suspension was mixed. The cell suspension was centrifuged at 800 rpm for 6 min. The supernatant was withdrawn and cells were resuspended with new medium (D-MEM (Dulbecco's Modified Eagle Medium-low glucose) (Sigma-Aldrich) with 10% (volume/volume) heat-inactivated bovine serum (Sigma-Aldrich), penicillin-streptomycin (10 units/mL and 10 mg/mL, respectively, Gibco), bovine insulin (5 μg/mL, Sigma-Aldrich), and glucose solution (2 mg/mL, Otsuka)). Cells were filtered with a 100 μm nylon cell strainer (Falcon). Dissociated and

filtered cells were seeded as mixed glia cultures in 75 cm^2 tissue flasks (Falcon) in D-MEM (Dulbecco's Modified Eagle Medium-low glucose) (Sigma-Aldrich) with 10% (volume/volume) heat-inactivated bovine serum (Sigma-Aldrich), penicillin-streptomycin (10 units/mL and 10 mg/mL, respectively, Gibco), bovine insulin (5 μg/mL, Sigma-Aldrich), and glucose solution (2 mg/mL, Otsuka) and cultured for 10 to 20 days at 37°C in a humidified CO_2 incubator until the cells were 100% confluent. Primary microglia were obtained by shaking the flasks containing the mixed glia cultures and the supernatant with floating cells. Floating cells (representing microglia) were seeded on 35 mm-diameter dishes containing 12 mm cover glasses (Matsunami Glass, 1082511226 not washed (hydrophilic)) at a density of 1 x 10^4 cells/dish and incubated at 37°C in a humidified CO_2 incubator for Patch clamp assays. Cells were seeded on 35 mm diameter dishes with a 14-mm glass bottom (Matsunami Glass, D1153OH) at a density of 1 x 10^4 cells/dish and incubated at 37°C in a humidified CO_2 incubator for Time-Lapse imaging. Cells were seeded on 35-mm diameter dishes containing 27-mm cover glasses (Matsunami Glass, D1114OH) at a density of 2 x 10^6 cells/dish and incubated at 37°C in a humidified CO_2 incubator for Patch clamp assays. Cells were used for experiments within 6 days of isolation.

2.3. Immunohistochemistry

The coverslips previously seeded with primary mouse microglia were fixed with 10% Formalin Neutral Buffer Solution (Wako, 062-01661) and incubated for 30 min on ice. Permeabilization was performed with 0.25% PBST (1X PBS + 100X TRITON (Sigma X100)). Blockage was performed with 1% BSA (Albumin, from Bovine Serum, IgG/Protease Free Wako 010-25783) diluted in 0.25% PBST. The first antibody (rabbit-anti-Iba-1 (WAKO 019-19741) was diluted at 1:500 in 1% BSA-0.25% PBST. Cells were incubated with the first antibody at 4°C overnight. After washing with blocking solution, the cells were incubated with the secondary antibody (goat anti-rabbit IgG (Molecular Probes Alexa Fluor 594, A-11037, diluted 1:1000)). Then, the cells

were labeled for 10 min with DAPI (Dojindo, FK0044, diluted 1:1000). Finally, cells were washed with PBS, sealed with Fluoromount (Diagnostic Biosystem KO24). Sealed coverslips were placed on the stage of an inverted Keyence BZ-9000 (Keyence) fluorescent microscope and image acquisition was performed using BZ-9000 software.

2.4. Cell Culture and Transfection

HEK293T cells were maintained in D-MEM (Wako) supplemented with 10% (volume/volume) fetal bovine serum (BioWest or Gibco), penicillin-streptomycin (50 units/mL and 50 μg/mL, respectively, Gibco) and GlutaMAX (2 mM, Gibco) and seeded at a density of 5 x 10^5 cells per 35-mm dish 24 h before transfection. For patch-clamp and cell volume change recordings, HEK293T cells cultured in OPTI-MEM I medium (Invitrogen) on 35-mm dishes were transfected with 0.7 μg expression vector and 0.1 μg pGreen-Lantern 1 cDNA (pGL1) using Lipofectamine (Invitrogen) and Plus reagents (Invitrogen) according to the manufacturer's protocol. After incubation for 3 to 5 h, cells were reseeded on cover glasses and further incubated at 37°C in a humidified CO_2 incubator. Cells were used for experiments 20 to 26 h after transfection.

2.5. Electrophysiology

Transfected HEK293T cells or primary mouse microglia on cover glasses were incubated in culture medium at 37°C ((D-MEM (Wako) supplemented with 10% (volume/volume) fetal bovine serum (BioWest or Gibco), penicillin-streptomycin (50 units/mL and 50 μg/mL, respectively, Gibco) and GlutaMAX (2 mM, Gibco) for HEK293T cells), (D-MEM (Dulbecco's Modified Eagle Medium-low glucose) (Sigma-Aldrich) with 10% (volume/volume) heat-inactivated bovine serum (Sigma-Aldrich), penicillin-streptomycin (10 units/mL and 10

mg/mL, respectively, Gibco), bovine insulin (5 μg/mL, Sigma-Aldrich), and glucose solution (2 mg/mL, Otsuka)) for primary mouse microglia). The cover glasses were washed with a standard bath solution containing 140 mM NaCl, 5 mM KCl, 2 mM $MgCl_2$, 2 mM $CaCl_2$, 10 mM HEPES, and 10 mM glucose at pH 7.4 (adjusted with NaOH). The cover glasses were mounted in a chamber (Warner Instruments) connected to a gravity flow system to deliver various drug stimuli and bath solutions. Recording pipettes were fabricated with a horizontal puller (Sutter Instruments, Model P-97). For experiments shown in Figure 4, we used a KCl intracellular pipette solution containing 140 mM KCL,10 mM HEPES, 5 mM EGTA and a range of Ca^{2+} from 0 to 10 μM at pH 7.4. For experiments shown in Figure 5, we used a KCl intracellular pipette solution containing 140 mM KCL,10 mM HEPES, 5 mM EGTA and 500 nM Ca^{2+} at pH 7.4. For Figure 5A, the intracellular pipette solution contained 140 mM KCL,10 mM HEPES, 5 mM EGTA and 100 μM ADPR. The extracellular solution was standard bath solution. For Figure 5B, the intracellular pipette solution remained the same as that in Figure 5A, but the extracellular solution was standard bath solution supplemented with 10 μM TRAM-34.

For the experiments on cell volume changes, the KCl intracellular pipette solutions used above were supplemented with 500 μM Calcein (Sigma-Aldrich, C0875).

For all the experiments in which the intracellular free-Ca^{2+} was fixed at 500 nM, 4.48 mM $CaCl_2$ was added (calculated by Webmaxc, standard version) before the pH was adjusted to 7.4.

For all the experiments in which the intracellular free-Ca^{2+} was fixed at 100 nM, 3.18 mM $CaCl_2$ was added before the pH was adjusted. Data for analysis were sampled at 10 kHz and filtered at 5 kHz for whole-cell recording (Axon Digidata 1550 amplifier with pClamp software, Molecular Devices). The membrane potential was clamped at -60 mV for all cell lines and mouse primary microglia. A ramp pulse protocol from -100 to +100 mV for 500 msec was applied every 5 sec. All experiments were performed at room temperature.

2.6. *In vitro* Time-Lapse imaging of microglia movement

Glass bottom dishes containing primary mouse microglia were placed on the stage of a Fluoview FV1200 (OLYMPUS) fitted with a temperature-controlled incubator (Tokai Hit) under a circulating mixture of gases (20% O_2, 5% CO_2, and 75% N_2). The stage/cover temperatures were set at 37/40°C (37°C) or 40/41°C (40 °C) for each experiment at least 1 h before cell image acquisition. The temperature setting for each condition was determined in advance by measuring the medium temperature with a wire probe and a digital thermometer (Unique Medical). Cells were imaged at 1 min intervals with a 20X phase contrast objective lens (Nikon Instech). Image acquisition was performed with Fluoview software with the Z-stack function. Focused images taken with the Z-stack function were automatically selected on ImageJ (NIH) in each frame correction and then reconstructed into a series of stacking image along the time axis. The migration distances of microglia were analyzed using ImageJ and the Manual Tracking and the Migration plugin tool. Excel software (Microsoft) was used to calculate the migration distances of individual cells. Data defining the migration distances of microglia were collected from at least four individual glass bottom dishes and four different preparations by analyzing all cells or randomly analyzing ≈30 cells per dish. Statistical analysis of motility was performed using the Wilcoxon/Kruskal-Wallis test followed by the Steel-Dwass method in JMP 14 software. *P* values less than 0.05 were considered significant.

2.7. Elisa Assay

Microglia were shaken off their co-culture layer, and plated at 5 x 10^5 cells per well in 24-well plates containing coated coverslips and microglia medium. Culture medium was changed 2 h later to 500 μL fresh microglial medium with 100 ng/mL LPS O26:B6 (Sigma-Aldrich), 10 μM TRAM-34 (Cayman Chemicals), or both or without drugs. Cells were incubated for 48 h at 37°C

in a humidified 5% CO_2 incubator. Supernatants were collected and used immediately for cytokine ELISA assay. Remaining samples were stored at -80°C pending future analysis.

Mouse IL-1β was assayed using ELISA kits purchased from R&D systems (Minneapolis, MN) according to the instructions provided by the manufacturer. Plates were read with a Thermo Scientific Labsystems 1500 Multiskan. Statistics for cytokine production was performed using a Wilcoxon/Kruskal-Wallis test followed by Steel-Dwass method on JMP 14 software. *P* values less than 0.05 were considered significant.

2.8. Chemicals

Stock solutions were prepared by dissolving TRAM-34 (Cayman Chemicals) in DMSO (Wako). ADPR (Sigma-Aldrich) was dissolved in MilliQ water (in order to get 100 mM ADPR), aliquoted and stored at -80°C pending future experiments. LPS O26:B6 were purchased from Sigma-Aldrich and diluted in MilliQ water (in order to get 100 µg/mL LPS), aliquoted and stored at -20°C pending future experiments. The aliquoted chemicals were diluted 1:1000 in the pipette solution patch-clamp (ADPR) or in the medium for ELISA and time-lapse imaging experiments, respectively. The final DMSO concentration did not exceed 0.1%.

2.9. Statistical analysis

Data are represented as means ± SEM. The distribution of data was first analyzed with the Shapiro-Wilk test. Statistical analysis was performed with Origin software (OrginLab) using a Student's t-test or ANOVA with a post hoc Bonferroni test for parametric data. For non-parametric data, statistical analysis was performed with JMP 14 software using a Wilcoxon/Kruskal-Wallis test followed by the Steel-Dwass method. *P* values less than 0.05 were considered significant.

3. Results

3. A. HEK293T cells

1. EC_{50} of $IK_{Ca}1$ in HEK293T cells

The EC_{50} values of $IK_{Ca}1$ for Ca^{2+} were determined in HEK293T cells by using different concentrations of Ca^{2+} in the pipette solution. The Ca^{2+} concentration range varied between 0 - 10 μM. Our EC_{50} values were around 450 nM (Figure 4), which agrees with a previous publication (Ledoux, J. et al., 2006), and is similar to the EC_{50} values for CaM (Shen, Y. et al., 2002). The similarities between $IK_{Ca}1$ and CaM EC_{50} are understandable because $IK_{Ca}1$ is activated following the binding of Ca^{2+} to the binding site of CaM which is entwined at its C-terminus (Figure 3). Accordingly, it was decided to use 500 nM Ca^{2+} in order to activate $IK_{Ca}1$ for all the experiments.

2. TRAM-34 is a specific inhibitor of the $IK_{Ca}1$ channel

1-[(2-Chlorophenyl)diphenylmethyl]-1H-pyrazole (TRAM-34) is a derivative of the azole anti-mycotic clotrimazole and has been shown to be a specific inhibitor of $IK_{Ca}1$. I tested the effect of TRAM-34 on $IK_{Ca}1$ expressed in HEK293T cells. After activation of $IK_{Ca}1$ channels with 500 nM Ca^{2+} contained inside the pipette solution, I applied 10 μM TRAM-34 extracellularly (Lallet-Daher. H. et al., 2009). TRAM-34 (10 μM) significantly inhibited the $IK_{Ca}1$ channels (p-value <0.05) (Figure 5 B-D).

This result is concordant with previous publications (Lallet-Daher, H., et al., 2009; Brown, B. M, et al., 2018) where the binding site of TRAM-34 was mentioned. TRAM-34 binds to the inner site of the P-Loop close to threonine 250 (T250) in all of the subunits and blocks K^+ ion conduction. At the same time, the pyrazole ring (containing the nitrogen) of TRAM-34 is

positioned between valine 275 (V275) located in the S6 and forms a hydrogen bond with the T250 of one of other subunits (Brown, B. M., et al., 2018). After activation by Ca^{2+}, $IK_{Ca}1$ channels appear desensitized, which is called “run-down” with high speed (Figure 5 A). This run-down has been explained in three ways: 1) the minimum Ca^{2+} threshold is achieved and all Ca^{2+} ions are already fixed on CaM present on $IK_{Ca}1$; 2) all the Ca^{2+}-binding sites are occupied by Ca^{2+} on CaM; 3) the activated $IK_{Ca}1$ channel closed automatically after being activated because the activation is temporary. At the present, there is no definitive explanation for the run-down observed on $IK_{Ca}1$ channels.

I next asked whether TRAM-34 had any effect on TRPM2, which is the second channel used to assess our hypothesis. For that, TRPM2-expressing HEK293T cells were pre-treated for 30 sec with 10 μM TRAM-34 before making a whole-cell configuration. TRPM2 is activated by 100 μM ADPR contained in the pipette solution (Eisfeld, J. and Luckhoff, A., 2007). The treatment with 10 μM TRAM-34 lasted for 1 min, after which the extracellular medium was washed out with 2 mM Ca^{2+} standard bath solution. Based on the results shown in (Figure 6 A-D), there was no inhibition of the TRPM2-mediated currents when treated with 10 μM TRAM-34 (CONTROL = 28.0 ± 6.8 nA vs. TRAM-34 treated = 31.7 ± 7.4 nA). This result indicated that TRAM-34 is a specific inhibitor of $IK_{Ca}1$ channels. This pharmacological tool can be used in order to discriminate K^+ currents induced by $IK_{Ca}1$ channels.

3. ADPR had no effect on the $IK_{Ca}1$ channel

To determine whether ADPR directly activated $IK_{Ca}1$ channels without Ca^{2+} intake, I did a patch-clamp experiment with a pipette solution containing 100 μM ADPR. $IK_{Ca}1$-mediated currents were not observed in the presence of ADPR in $IK_{Ca}1$-expressing HEK293T cells or in mock cells transfected with pcDNA3.1 alone (Figure 6 D-H). The mean normalized peak current

density of IKCa1 channels at -60 mV was approximately 0.8 ± 0.1 pA/pF, which was similar to those obtained in mock cells (0.8 ± 0.1).

4. Ca^{2+} influx induced by ADPR-activated TRPM2 activated the $IK_{Ca}1$ channel in co-transfected HEK293T cells

In HEK293T cells co-expressing TRPM2 and $IK_{Ca}1$ channels, I established a representative current trace (Figure 7 A). ADPR (100 μM) contained in the pipette solution activated TRPM2 channels. The ADPR-activated current was 27.3 ± 7.0 pA/pF at a membrane potential of -60 mV with a linear current-voltage (IV) relationship (Figure 7 C). Those results are typical for the early stage of activation of TRPM2 (Luo, X. et al., 2018). The reversal potentials (E_{rev}) were = -19.1 ± 2.3 mV (Figure 7 E). As predicted in our hypothesis, Ca^{2+} entering the cell via TRPM2 bound to CaM and activated the $IK_{Ca}1$ channels. Mean peak current density was 2.1 ± 13.2 pA/pF at -60 mV and E_{rev} values were shifted toward -56.8 ± 2.9 mV (Figure 7 E). Activation of $IK_{Ca}1$ channels could explain the shift of E_{rev} toward negative values.

It is important to note that after the activation of the $IK_{Ca}1$ channels, I observed peak currents (values = -367.6 ± 67.1 pA/pF) that likely reflected the maximal activation of TRPM2. Moreover, the E_{rev} values were shifted toward -29.0 ± 4.3 mV (Figure 7 A, C, E). These data indicated that both TRPM2 and $IK_{Ca}1$ channels were activated.

To be certain that $IK_{Ca}1$ was activated by the TRPM2-induced calcium influx, I specifically inhibited the channel with 10 μM TRAM-34. I observed that the currents (120 sec after the peak) were significantly smaller in cells treated with 10 μM TRAM-34 (= -37.2 ± 9.7 pA/pF) compared to non-treated cells (= 28.5 ± 20.0 pA/pF) (Figure 7 B, D) (p-value <0.001). Likewise, the E_{rev} values were also significantly different between cells treated with 10 μM TRAM-34 and non-treated cells (Figure 7 B, D, E) (p-value <0.001). E_{rev} values were -62.2 ± 3.1 mV for non-treated cells, whereas E_{rev} values were -25.2 ± 4.6 mV in TRAM-34-treated cells. The E_{rev}

values 120 sec after the peak in TRAM-34-treated cells were close to the E_{rev} values of the possible initial TRPM2-mediated currents. My interpretation is that $IK_{Ca}1$ was almost completely inhibited, and only TRPM2-mediated currents were observed.

5. $IK_{Ca}1$ activation induces shrinkage of HEK293T cells

The increases in K^+ efflux through $IK_{Ca}1$ might have been accompanied by water efflux, a process that would reduce the cells' volume. Therefore, I examined the cells' volume changes during the whole-cell patch-clamp experiments under different conditions. First, I compared $IK_{Ca}1$-expressing cells and pcDNA3.1-transfected (mock) cells with 500 nM Ca^{2+} contained in the pipette solution. After making a whole-cell configuration in cells expressing $IK_{Ca}1$, there was a 22 ± 2 % reduction in cell volume after 5 min and a 35 ± 3 % reduction after 10 min. Those values were significantly larger than those in mock cells (Figure 8 A-C) (p-value <0.001). To verify that the volume reduction was due to $IK_{Ca}1$ channel activation by the Ca^{2+} contained in the pipette solution, I pre-treated $IK_{Ca}1$-expressing cells with 10 μM TRAM-34. Cell shrinkage was abolished in the TRAM-34-pre-treated cells and cell volumes were significantly different from those in the non-treated $IK_{Ca}1$-expressing cells (Figure 8A-C) (p-value <0.001).

Then, I analyzed cells co-expressing TRPM2 / $IK_{Ca}1$ channels with 100 μM ADPR contained in the pipette solution. Shrinkage values were 27 ± 4 % after 5 min and 40 ± 3 % after 10 min after making a whole-cell configuration, which was significantly larger than mock cells (Figure 8 B-D) (p-value <0.001) or cells transfected with TRPM2 alone (p-value <0.001). Taking these data together, these results enabled us to conclude that activation of the $IK_{Ca}1$ channel induced K^+ efflux, followed by a flow of H_2O from the cytosol toward the extracellular medium. (Figure 8). These results agree with previous publications that stated that the flow of K^+ is accompanied by Cl^- and water efflux decreasing cell volume (Hayabuchi, Y. et al., 2017; Takayama, Y. et al., 2014).

3. B. Mouse primary microglia

1. Purity of isolated mouse primary microglia

In order to confirm that the interaction between TRPM2 and $IK_{Ca}1$ also occurred in native cells, I examined microglia, which are known to express both TRPM2 and $IK_{Ca}1$. After isolating the microglial, I tested the purity of these cells. The microglia were labeled with an anti-Iba-1 antibody. Iba-1 (ionized calcium-binding adapter molecule 1) is a well-known marker for microglial identification (Hopperton, K. E. et al., 2018; Jurga, A. M. et al., 2020). Labeled cells were examined to determine their purity (Figure 9 A-B). The purity of the cell culture was 98% (Figure 9 C), in agreement with a previous publication (Doering, L. C., 2010; Nishimoto, R. et al., 2021; Yildizhan, K. et al., 2020).

2. Activation of TRPM2 by ADPR (with 100 nM Ca^{2+}) induced an influx of Ca^{2+} that activated $IK_{Ca}1$ in mouse primary microglia

I found that a pipette solution containing 100 μM ADPR alone activated TRPM2 in wild-type (WT) microglia (peak current densities of WT vs. TRPM2 KO were significantly different; p-value <0.001). However, the Ca^{2+} entering the cell through the TRPM2 channels was insufficient to activate $IK_{Ca}1$ (Figure 10) (Ferreira, R. and Schlichter, L. C., 2013; Kacik, M. et al., 2014). Upon making a whole cell configuration, I did not observe a shift of E_{rev} towards negative E_{rev} values expected for $IK_{Ca}1$ activation (E_{rev} values were -4.9 ± 1.1 mV in WT cells and -8.8 ± 1.9 mV in TRPM2 KO cells after 5 sec. In comparison, values were -12.1 ± 2.1 mV in WT cells and -13.2 ± 2.5 mV in TRPM2 KO cells 90 sec after making a whole-cell configuration) (Figure 10).

It was possible that the Ca^{2+} threshold to activate $IK_{Ca}1$ channel was not achieved under the

experimental condition. Consequently, I supplemented the 100 μM ADPR pipette solution with 100 nM Ca^{2+}. I observed again the activation of TRPM2-mediated currents (E_{rev} = -17.2 ± 2.3 mV) the peak of which was significantly larger than the currents in TRPM2 KO cells (Figure 11 A, B) (p-value<0.001). E_{rev} values were shifted towards -56.1 ± 2.2 mV after 90 sec in a whole-cell configuration (Figure 11 A, B). In comparison, at this same time point, I did not observe a shift in TRPM2 KO cells and the E_{rev} values were -12.2 ± 2.2 mV, which was significantly different from the values in WT cells E_{rev} (p-value <0.001) even 5 min after making a whole-cell configuration (Figure 10 D).

In the next step, I used WT microglia in the presence of 10 μM TRAM-34 in order to verify that this shift of E_{rev} values was due to activation of $IK_{Ca}1$ channels. Possible activation of TRPM2 was still observed in the presence of TRAM-34 (peak current densities in WT cells were -64,9 ± 10.8 pA/pF and 37.7 ± 8.1 pA/pF at -60 mV with or without TRAM-34, respectively). $IK_{Ca}1$ activation seemed to be inhibited, as revealed by the changes in E_{rev} values (E_{rev} values were -13.4 ± 1.9 mV and -56.1 ± 2.2 mV with or without TRAM-34, respectively, 90 sec after making a whole-cell configuration (p-value <0.001)). The values were significantly different (p-value <0.001) even at 5 min (-16.1 ± 2.0 mV and -48.3 ± 3.9 mV with or without TRAM-34, respectively) (p-value <0.001). To be sure that the shift observed in (Figure 11A) was derived from $IK_{Ca}1$ channel activation, an additional control experiment was performed. I directly activated $IK_{Ca}1$ channels in TRPM2 KO mouse primary microglia with 500 nM Ca^{2+} in the KCl pipette solution. I observed (Figure 11E) that 500 nM Ca^{2+} directly activated $IK_{Ca}1$ channels in TRPM2 KO mouse primary microglia, and the E_{rev} values were characteristic for $IK_{Ca}1$ activation (E_{rev} values were -66.4 ± 3.1 mV and E_{rev} = -16.3 ± 1.7 mV without or with TRAM-34 at 5 sec, respectively, and -62.6 ± 4.6 mV and -19.5 ± 2.3 mV without or with TRAM-34 at 90 sec after making a whole-cell configuration, respectively.

3. Cell volume changes in a TRPM2-$IK_{Ca}1$-dependent manner occurred in mouse primary microglia

To assess volume changes in mouse primary microglia, I examined volume changes as previously done for HEK293T cells. During patch-clamp experiments, I added 500 μM Calcein to the pipette solution. First, I compared WT and TRPM2 KO microglia activated by 100 μM ADPR contained in the pipette solution. I noted (Figure 12 A-D) that once TRPM2 was activated by ADPR, WT primary mouse microglia shrank by around 21 ± 5 % at 5 min (p-value <0.001) and 36 ± 6 % at 10 min (p-value <0.001). The decrease in volume was not observed when I repeated the same experiments with TRPM2 KO primary microglia (Figure 12 B-D). Moreover, the shrinkage of WT primary mouse microglia was abolished when pre-treated extracellularly with 10 μM TRAM-34, both at 5 min and 10 min (p-values <0.001) (Figure 12 C, D), meaning that cell volume changes were due to activation of the $IK_{Ca}1$ channel as previously observed in HEK293T cells. To confirm that the cell volume changes were indeed due to the activation of $IK_{Ca}1$ channels, I used TRPM2 KO primary mouse microglia and directly activated $IK_{Ca}1$ channels with 500 nM Ca^{2+} in the pipette solution. The cells shrank by around 20 ± 1 % at 5 min (p-value <0.001) and 37 ± 2 % at 10 min (p-value <0.001) after making a whole-cell configuration in cells without TRAM-34 (Figure 12 E-G).

Taken together, these data indicated the following events. TRPM2 was activated by ADPR and Ca^{2+} entered the cells. The Ca^{2+} then activated $IK_{Ca}1$ channels that in turn allowed K^+ efflux. The K^+ efflux induced significant cell volume changes in mouse primary microglia. These results are consistent with our previous data observed in HEK293T cells and previous analyses of the flow of K^+ in which it was accompanied by Cl^- and water efflux and a decrease in cell volume (Hayabuchi. Y. et al., 2017; Takayama, Y. et al., 2014).

4. Microglia exhibited temperature- and TRPM2-$IK_{Ca}1$-dependent movement

The cell volume changes suggested that there might be a link with cell migration. Cell migration can be described as a repetitive cycle of protrusion of the cell front that is followed by retraction of the tail part. In terms of cell volume, this cycle can be modelled as volume gain at the cell front and volume loss at the rear of migrating cells. This view is also supported by the observation that the protrusion of the lamellipodium and the retraction of the tail part do not always occur simultaneously in migrating cells (Schwab, A. et al., 2012). Rather, one of these processes temporarily dominates. Cell volume could increase during the protrusion of the lamellipodium whereas it decreases during the retraction of the tail portion (Figure 13) (Schwab, A. et al., 2012).

Furthermore, a local volume decrease up to 35% has been visualized in migrating cells in previous publications (Happel, P. et al., 2010; Schneider, S.W. et al., 2000; Watkins, S., and Sontheimer, H., 2011). These values are similar to the values observed in my experiments, i.e., 37% (Figure 12).

To asses this hypothesis, I performed time-lapse imaging of WT and TRPM2 KO microglia at 37°C and 40°C. The distance traveled by microglia was significantly larger at 40°C (176.1 ± 5.1 μm) than 37°C (131.9 ± 5.1 μm) (p-value <0.001) (Figure 14), meaning that WT primary mouse microglia exhibited temperature-dependent movement as I found before (Nishimoto. R. et al., 2021). The temperature-dependent movement was lost when cells were pre-treated with 10 μM TRAM-34 both at 37°C (97.3 ± 4.1 μm) (p-value < 0.001) and 40°C (112.4 ± 4.0 μm) (p-value < 0.001) (Figure 14).

I also observed that TRPM2 KO microglia showed less movement compared to WT microglia both at 37°C (95.5 ± 4.2 μm) and 40°C (126.7 ± 4.3 μm) (p-value <0.001) (Figure 14). However, even with TRPM2 KO cells, the pre-treatment with 10 μM TRAM-34 decreased the cell travel

distance compared to non-treated microglia at 37°C (63.5 ± 3.8 μm) (p-value<0.001). Results appeared to be similar at 40°C, although the difference in distances was not statistically significant (126.7.1 ± 4.3 μm and 100.1 ± 3.9 μm without or with TRAM-34). This result suggested that even in TRPM2 KO cells, $IK_{Ca}1$ channels could be activated by Ca^{2+} through other sources such as CRAC (Wulff, H. and Castle, N. A., 2010; Maezawa, I. et al., 2012) and ORAI-STIM (Kraft, R., 2015).

These data suggested that the TRPM2 / $IK_{Ca}1$ channel network contributes to mouse primary microglia movement. Furthermore, this motility is impaired when one of these channels was deleted or inhibited.

5. TRAM-34 treatment reduced IL-1β cytokine production in WT and TRPM2 KO mouse primary microglia

In previous publications, it was shown that both TRPM2 and $IK_{Ca}1$ channels contributed to Il-1β production (Kashio, M., et al., 2012; Nguyen, H. M., et al., 2017). However, the contribution of the TRPM2 / $IK_{Ca}1$ network has not been described. Thus, I investigated whether the TRPM2 / $IK_{Ca}1$ network contributed to Il-1β production in mouse primary microglia. I first determined an effective concentration of LPS for mouse primary microglia. A dose of 100 ng/mL was adequate based on a protocol in the literature (Figure 15).

Microglia stimulated with 100 ng/mL LPS showed a significant increase in the release of Il-1β in the medium compared to the control (Figure 15) (p-value <0.001). A significant increase was also observed in 100 ng/mL LPS-stimulated TRPM2 KO microglia compared to the control (Figure 15) (p-value <0.001) although the magnitude of the increase was significantly less in the TRPM2 KO microglia compared to WT cells (Figure 15) (p-value <0.001). These data suggested that TRPM2 mediated Il-1β production in microglia, in agreement with a previous publication (Kashio, M., et al., 2012). Then, in order to investigate whether $IK_{Ca}1$ channels were also

involved in the Il-1β production pathway, I stimulated WT and TRPM2 KO microglia with 100 ng/mL LPS in the presence of 10 μM TRAM-34 (Figure 15). I observed that LPS-induced Il-1β production was almost completely abolished when $IK_{Ca}1$ channels were blocked by TRAM-34 in WT and TRPM2 KO mouse primary microglia (p-value <0.001). Together, these data suggested that LPS-induced Il-1β production requires a TRPM2 / $IK_{Ca}1$-dependent pathway in mouse primary microglia.

4. Discussion

TRPM2 and $IK_{Ca}1$ channels are widely studied as separate entities, and their interaction has not been shown previously. In the present study, I aimed to determine whether TRPM2 interacted with the $IK_{Ca}1$ channel and if this network contribute to any physiological processes. I confirmed that ADPR is an agonist of TRPM2 and that TRAM-34 is a specific inhibitor of $IK_{Ca}1$. I co-expressed both channels in HEK293T cells in order to assess whether TRPM2 / $IK_{Ca}1$ channels interacted with each other. HEK293T cells are commonly used as tools to investigate the function of ion channels because of the low-level expression of transporters and ion channels (Gao, J. et al., 2005). Using a patch-clamp method (Figure 6), I clearly showed that ADPR activated the TRPM2 channel. It is believed that once the TRPM2 channel is activated, Ca^{2+} enters the cell from the extracellular part and moves into the interior. After Ca^{2+} binding to CaM, this interaction activates the $IK_{Ca}1$ channel and induces K^+ efflux. Activation of $IK_{Ca}1$ channels induced a shift of E_{rev} values (Figure 7) accompanied by a cell volume change in HEK293T cells (Figure 8). Upon activation of the $IK_{Ca}1$ channel by Ca^{2+} entering the cell through TRPM2 or directly with 500 nM of intracellular Ca^{2+}, I observed reductions in cell volume from 35% to 40% in HEK293T cells. These data agreed with a previous analysis in which K^+ efflux induced by the $IK_{Ca}1$ channel was followed by Cl^- and water efflux from the cytosol and a consequent decrease in cell volume (Hayabuchi, Y. et al., 2017; Takayama, Y. et al., 2014). It should be noted that voltage-independent Cl^- channels (Yu, S. P. and Kerchner, G. A., 1998) and water channels (Gao, J. et al., 2005) are expressed in HEK293T cells. These findings suggest that Ca^{2+} enters through TPRM2 or that K^+ efflux through $IK_{Ca}1$ may also trigger endogenous channels. In the future, it would be interesting to determine which Cl^- and water channels are involved in cell volume changes in HEK293T cells.

The data that I obtained with HEK293T cells permitted me to determine whether this network

was functional in primary cells and to identify the physiological processes in which it participated. Towards that end, I conducted a literature search to determine which cell types expressed both TRPM2 and $IK_{Ca}1$. According to the literature, these channels are expressed in vascular smooth muscle cells (Hayabuchi, Y. et al., 2017; Zhao, Q. et al., 2020), CA1 pyramidal neurons (King, B. et al., 2015; Olah, M. E. et al., 2009) and microglia (Brown, B. M., et al., 2018 and 2019; Sita, G. et al., 2018; Bouhy, D. et al., 2011). I focused on microglia because they constitute a primary innate immune population in the CNS and they are capable of migration, proliferation and phagocytosis (Marin-Teva, J. L. et al., 2011). Furthermore, I thought that cell volume changes previously observed in HEK293T cells could be linked to the migration of microglia. Also important, TRPM2 and $IK_{Ca}1$ channels independently participate in cytokine production (Kashio, M., et al., 2012; Nguyen, H. M., et al., 2017).

I first assessed the purity of microglia intended for experimentation (Figure 9). Finding it sufficient, I then performed patch-clamp experiments with primary mouse microglia to determine whether the results would be similar to those I previously observed in HEK293T cells. I determined that TRPM2 / $IK_{Ca}1$ interaction was present in primary mouse microglia. However, I supplemented pipette solution with 100 nM Ca^{2+} in order to achieve the physiological Ca^{2+} concentration of mouse primary microglia. Indeed, if the pipette solution contained only 100 μM ADPR, I observed TRPM2 activation, but not $IK_{Ca}1$ activation. In other words, the Ca^{2+} flux entering through TRPM2 was inadequate to reach the Ca^{2} thresholds needed for $IK_{Ca}1$ channel activation (Figure 10). This is the reason for using a pipette solution supplemented with 100 nM Ca^{2+} (Ferreira, R. and Schlichter, L. C., 2013; Kacik, M. et al., 2014). I observed that ADPR activated the TRPM2 channel. The activation of this channel likely induces Ca^{2+} influx into mouse primary microglia. Thus, Ca^{2+} together with the 100 nM Ca^{2+} permitted the ion to reach the Ca^{2+} thresholds needed for $IK_{Ca}1$ activation. Once $IK_{Ca}1$ was activated, a shift of E_{rev} values toward -56 mV was observed, meaning K^{+} efflux. At this point, the E_{rev} values were lower

compared with the theoretical values calculated with a Nernst equation (Equation A). The difference in the E_{rev} values could be partly explained by the function of endogenous Cl^- channels in microglia (Kolesnikov, D. et al., 2021; Cojocaru, A. et al., 2021; Skaper, S. T. et al., 2013; Kacik, M. et al., 2014; Ducharme, G. et al., 2007; Hines, D. J. et al., 2009; Thei, L. et al., 2018).

I observed that the activation of $IK_{Ca}1$ channel led to cell volume changes in microglia (Figure 12). I observed 36% cell shrinkage in WT microglia when the TRPM2 / $IK_{Ca}1$ network was triggered by 100 μM ADPR, and 37% cell shrinkage in TRPM2 KO microglia when $IK_{Ca}1$ was directly activated with 500 nM intracellular Ca^{2+}. I hypothesized that the flow of K^+ was accompanied by Cl^- and water efflux that decreased cell volume (Hayabuchi, Y. et al., 2017; Takayama, Y. et al., 2014). These data also support my previous idea in which the action of endogenous Cl^- channels explains the difference in the E_{rev} values.

Previously, cell migration was described as a repetitive process in which volume was gained in the front part of the cell and lost in the rear portion (Schwab, A. et al., 2012). Thus, I wondered if the volume changes observed in microglia might be linked to microglia movement. This concept is supported by the observation that the protrusion of the lamellipodium and the retraction of the tail part do not always occur simultaneously in migrating cells. Rather, one of these processes temporarily dominates. This suggests that the cell volume increases during the protrusion of the lamellipodium, whereas it decreases during the retraction of the tail part (Schwab, A. et al., 2012). Local volume changes in the previous publication were up 35% (Happel, P. et al., 2010; Scheinder, S.W. et al., 2000; Watkins, S. and Sontheimer, H. 2011), similar to the 37% shrinkage of primary microglia observed here (Figure 12). Those data support the idea that the volume changes could be linked to cell migration. My data agree with our previous study in which we showed that WT mouse primary microglia exhibit temperature-dependent movement (Nishimoto,

R. et al., 2021). Our team also reported that TRPM2 deficiency impaired temperature-dependent movement of mouse primary microglia (Nishimoto, R. et al., 2021). In this study, I found that temperature-dependent changes in movement in WT mouse primary microglia occurred through the TRPM2 / $IK_{Ca}1$ network. When $IK_{Ca}1$ was blocked by TRAM-34, there was no K^+ efflux that impaired Cl^- efflux and prevented water efflux. Those processes hinder the extension-retraction cycle and inhibit cell movement. However, temperature-dependent changes in the movement were also observed in TRPM2 KO primary mouse microglia, suggesting that $IK_{Ca}1$ is still activated while the changes were smaller than in WT. Other channels like CRAC (Wulff, H., and Castle, N. A., 2010; Maezawa, I., et al., 2012) or ORAI-STIM (Kraft, R., 2015) expressed in microglia could increase the intercellular Ca^{2+} concentrations. Nevertheless, Ca^{2+} influx through TRPM2 seems to be the most important activator of $IK_{Ca}1$.

There is another question regarding cell migration. It was mentioned that depolarization of the cell membrane potential exerts a modulatory effect on the cytoskeleton (Szaszi, K. et al., 2004; Waheed, F. et al., 2010). Indeed, it was shown that depolarisation of the membrane activates the ERK ➔ GTP/GDP exchange factor GEF-H1 ➔ Rho ➔ Rho-kinase system, leading to myosin light chain phosphorylation (Szaszi, K. et al., 2004; Waheed, F. et al., 2010). However, the relationship between $IK_{Ca}1$ and cytoskeleton polymerisation/depolymerization remains unclear. Is it only due to membrane depolarisation? Is it possible that the cytoskeleton senses the intracellular loss of K^+? Are there other intracellular proteins acting as mediators between $IK_{Ca}1$ and the cytoskeleton? Further studies are necessary to address these questions.

Finally, I wondered if the TRPM2 / $IK_{Ca}1$ network had a role in cytokine production. Microglia are described as a specialized population of primary innate immune cells in the CNS (Marin-Teva, J. L. et al., 2011). Thus, I investigated the ability of microglia to produce Il-1β. It was already shown that both TRPM2 and $IK_{Ca}1$ had separate roles in cytokine production (Kashio, M., et al., 2012; Nguyen, H. M., et al., 2017). In this study, I showed that WT and

TRPM2 KO microglia treated with 100 ng/mL LPS released significantly more Il-1β into the medium than did the control (Figure 15). However, LPS induced less Il-1β production in TRPM2 KO microglia compared to WT microglia. Finally, I observed that Il-1β production was abolished in cells co-treated with LPS and TRAM-34 (Figure 15). These data suggest that LPS-treated mouse primary microglia produced Il-1β in a TRPM2-I / $K_{Ca}1$-dependent manner. I speculate that the production of Il-1β may occur after the NLR family pyrin domain containing 3 (NLRP3) senses the K^+ efflux following $IK_{Ca}1$ activation (He, Y. et al., 2016). Unfortunately, the molecular mechanism leading to NLRP3 activation in response to K^+ efflux remains unknown. However, NEK7 proteins (NIMA-related kinase) act as NLRP3-binding proteins downstream of K^+ efflux (He, Y. et al., 2016; Chen, Y. et al., 2019). Positive regulation of NLRP3 leads to the activation of caspase-1 and maturation of Il-1β (He, Y. et al., 2016) (Figure 16).

In the future, I plan to perform two-photon imaging *in vivo* using WT and TRPM2 KO mice in order to investigate whether cytokine production is associated with microglia motility. Overall, my study has shown that TRPM2 and $IK_{Ca}1$ interact with one another. This finding helps us to understand different microglial processes working downstream from the TRPM2 / $IK_{Ca}1$ network. By understanding the mechanisms of microglia movement and cytokine production, and understanding how these phenotypes are modulated by temperature, we can identify new approaches to the treatment of CNS pathologies.

5. Figures and Legends

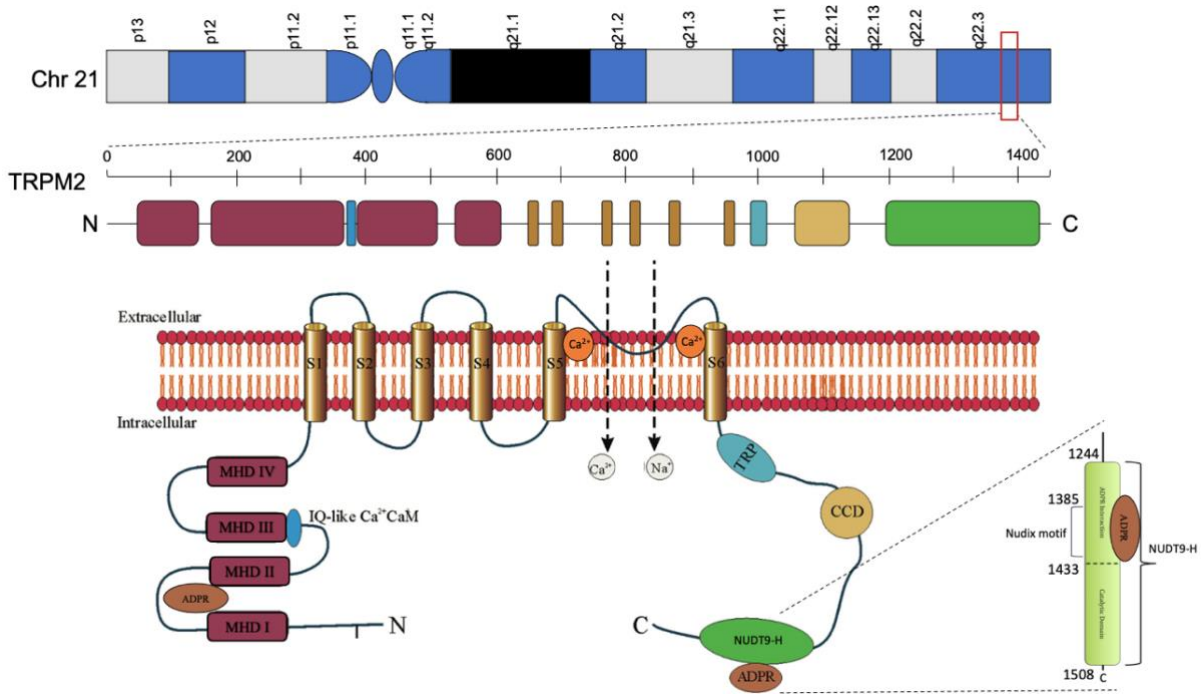

Figure 1. Schematic representation of the *TRPM2* gene and its transmembrane topology.

The human chromosome 21 schematic at the top shows the location of the *TRPM2* gene localized in the q22.31 locus. The full-length of the protein is composed of 1503 amino acids. Segments in the N terminus MHD I/II/III and IV regions followed by six transmembrane domains (S1-S6) with the pore forming region located between S5 and S6. The C-terminal region contains a TRP Box domain (hydrophobic and highly conserved region among TRP channels) located downstream of the pore region, coiled-coil motif (CCD) and NUDT9-homology region (NUDT9-H). The membrane topology of TRPM2 shows that both N-and C-termini are in the cytosol. ADPR binds to the NUDT9-H region and the MHD I/II region to induce channel gating and enable Ca^{2+} and Na^{+} influx.

Figure modified from Cheung, J.Y and Miller, B.A, 2017 with permission

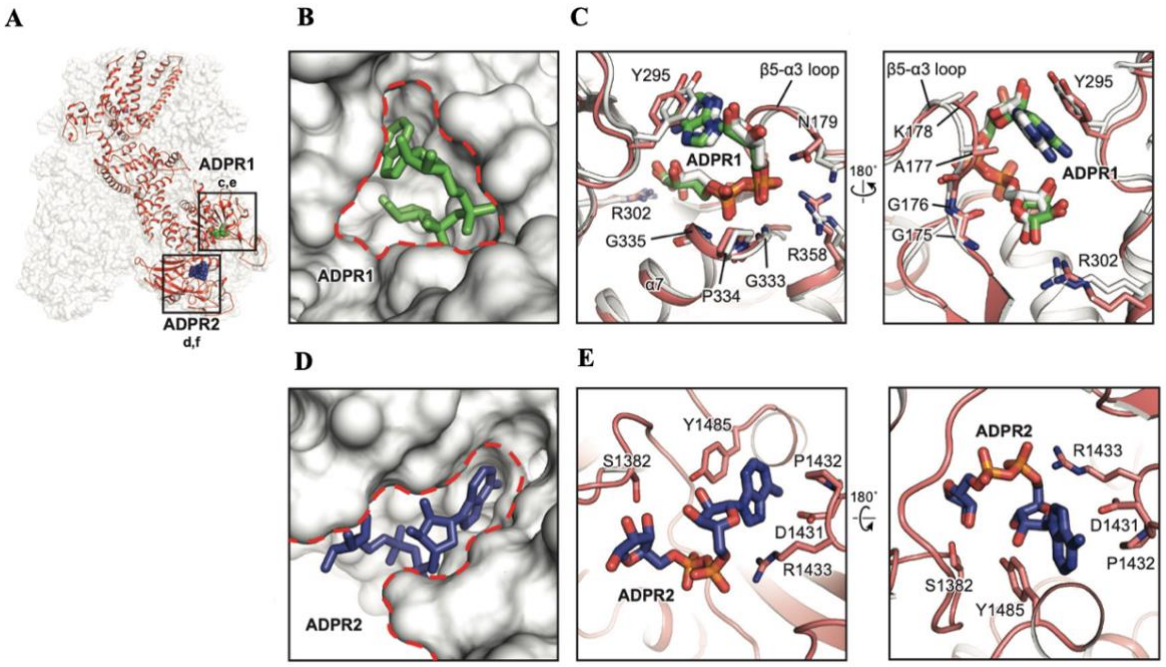
A
ADPR1
c,e
ADPR2
d,f
B
ADPR1
C
Y295
β5-α3 loop
N179
ADPR1
R302
G335
R358
α7
P334
G333
180°
β5-α3 loop
Y295
K178
A177
ADPR1
G176
G175
R302
D
ADPR2
E
Y1485
S1382
P1432
D1431
R1433
ADPR2
180°
ADPR2
R1433
D1431
P1432
S1382
Y1485

Figure 2. The ligand-binding site of the MHDI/II domain and NUDT9-H for ADPR. Shape changes occurring on APDR improves binding for this specific domain

(A) Location of both binding sites of ADPR on TRPM2. (B) Shape of ADPR on MHDI/II located at the N-terminal, which is the main binding site for this molecule. (C) Ligand-binding of ADPR on MHDI/II. D) Shape of ADPR on NUDT9-H domain located at the C-Terminus.
(E) Ligand-binding of ADPR on NUDT9-H domain.
Figure modified from Huang, Y et, 2019 with permission.

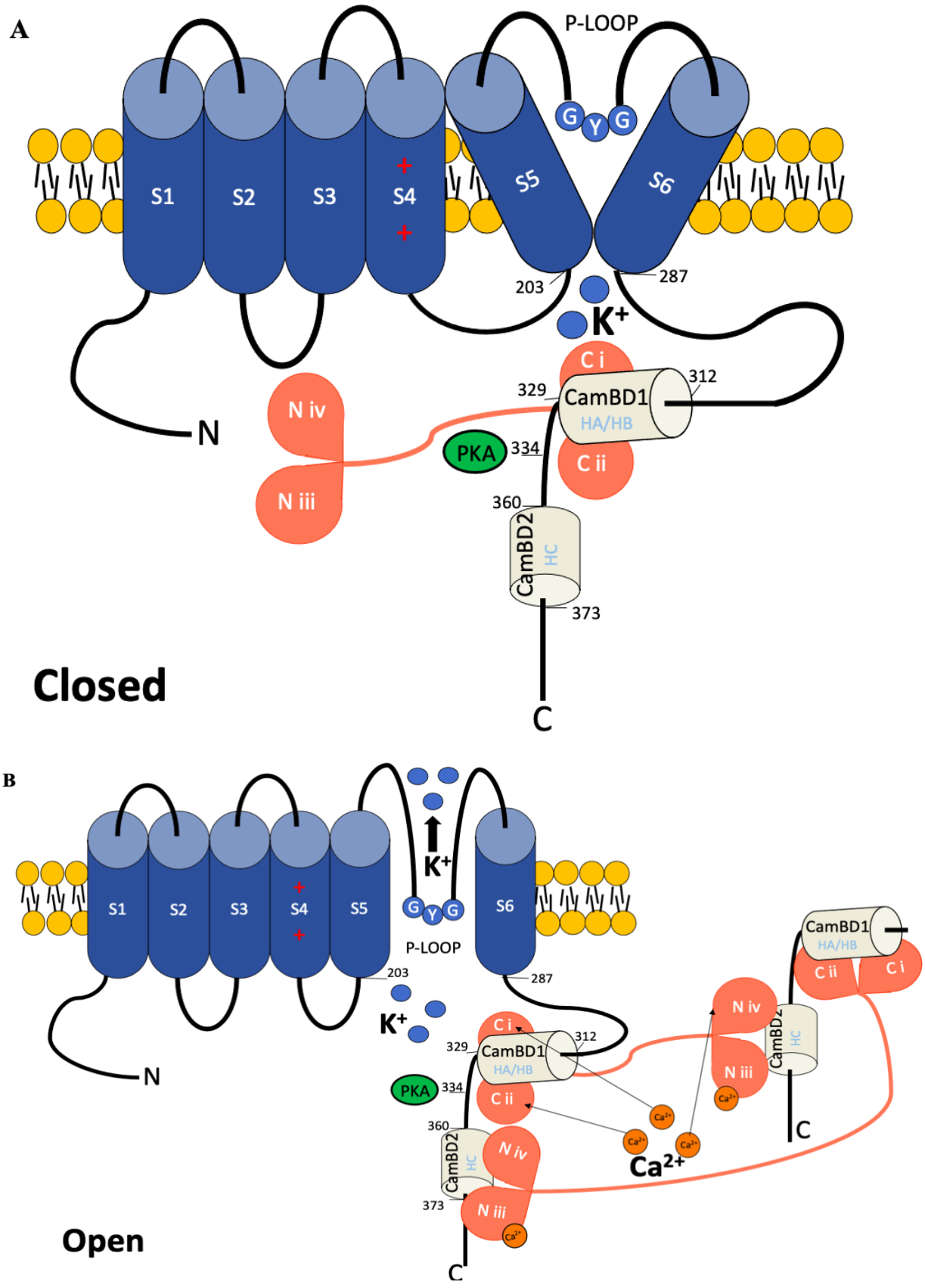
A
P-LOOP
G
Y
G
S1
S2
S3
S4
S5
S6
203
287
K+
C i
312
329
CamBD1
HA/HB
N iv
PKA
334
C ii
N iii
360
CamBD2
HC
373
N
C
Closed
B
K+
S1
S2
S3
S4
S5
G
Y
G
S6
P-LOOP
203
287
K+
N
C i
312
329
CamBD1
HA/HB
PKA
334
C ii
360
CamBD2
HC
N iv
373
N iii
Ca2+
CamBD1
HA/HB
C ii
C i
N iv
CamBD2
HC
N iii
C
Open

Figure 3. Transmembrane topology of the intermediate conductance calcium-activated potassium channel, $IK_{Ca}1$

Structure and transmembrane topology of intermediate conductance calcium-activated potassium channel $IK_{Ca}1$. Six TMD (S1-S6) constituting $IK_{Ca}1$ and prolonged by cytoplasmic N and C termini constitute each of the four-monomer forming $IK_{Ca}1$ channel. S4 carrying two arginines that give this a positive charge but not enough for voltage dependence. The P-Loop composing the pore domain of $IK_{Ca}1$ located between S5 and S6 have a GYG consensus sequence that is a potassium-selective filter. CaM is bent to CaM binding domain (CamBD1 HA/HB) by the C-lobes.

(A) In the absence of calcium. If the Ca^{2+} threshold in the cell is low, the N-lobes of CAM are free and positioned near to S2 and S3 intracellular segments. (B) In the presence of calcium. If the Ca^{2+} threshold in the cell is reached, the iii Ca^{2+}-binding site located on N-lobes of CaM will bind Ca^{2+} and induce a conformational change of CaM that allows the fixation of Ca^{2+} to the other site also. This conformational change of CaM also induces pulling by the C-terminal because CaM will bind to CamBD2 HC of another subunit of $IK_{Ca}1$. This change induces opening and potassium flux of $IK_{Ca}1$ from the intracellular region toward the extracellular compartment.

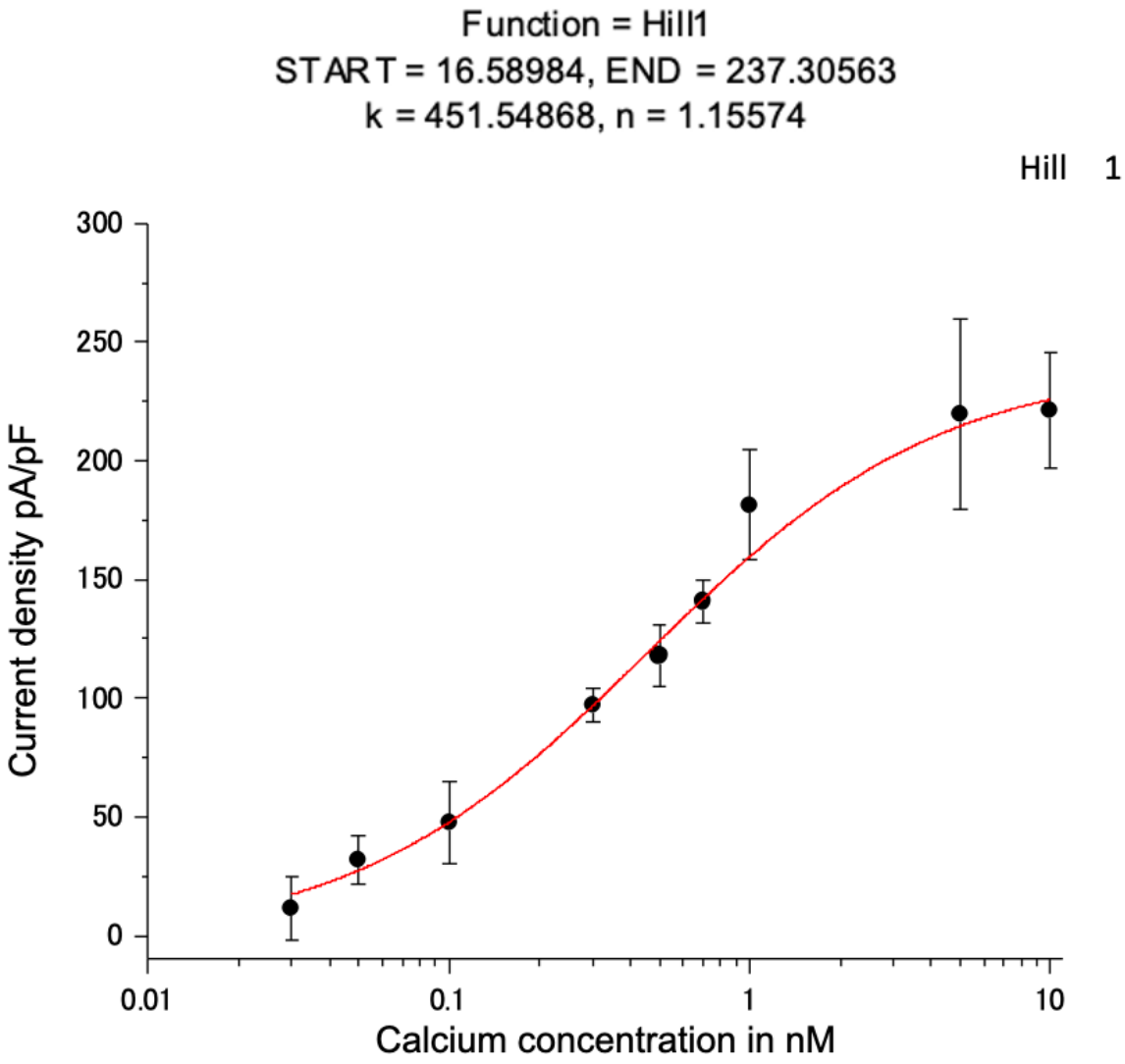
Function = Hill1
START = 16.58984, END = 237.30563
k = 451.54868, n = 1.15574
Hill 1
Current density pA/pF
300
250
200
150
100
50
0
0.01
0.1
1
10
Calcium concentration in nM

Figure 4. EC_{50} of the $IK_{Ca}1$ channel for Ca^{2+}

The EC_{50} for $IK_{Ca}1$ activation by defined intracellular Ca^{2+} concentration. Data was fitted with a Hill function using Origin software. Ca^{2+} range contained in pipette solution and independent trials number n: Ca^{2+} free (n = 14), 30 nM Ca^{2+} (n = 8), 50 nM Ca^{2+} (n = 9), 100 nM Ca^{2+} (n = 8), 300 nM Ca^{2+} (n = 10), 500 nM Ca^{2+} (n = 13), 700 nM Ca^{2+} (n = 6), 1 μM Ca^{2+} (n = 12), 5 μM Ca^{2+} (n = 11), 10 μM Ca^{2+} (n = 5),

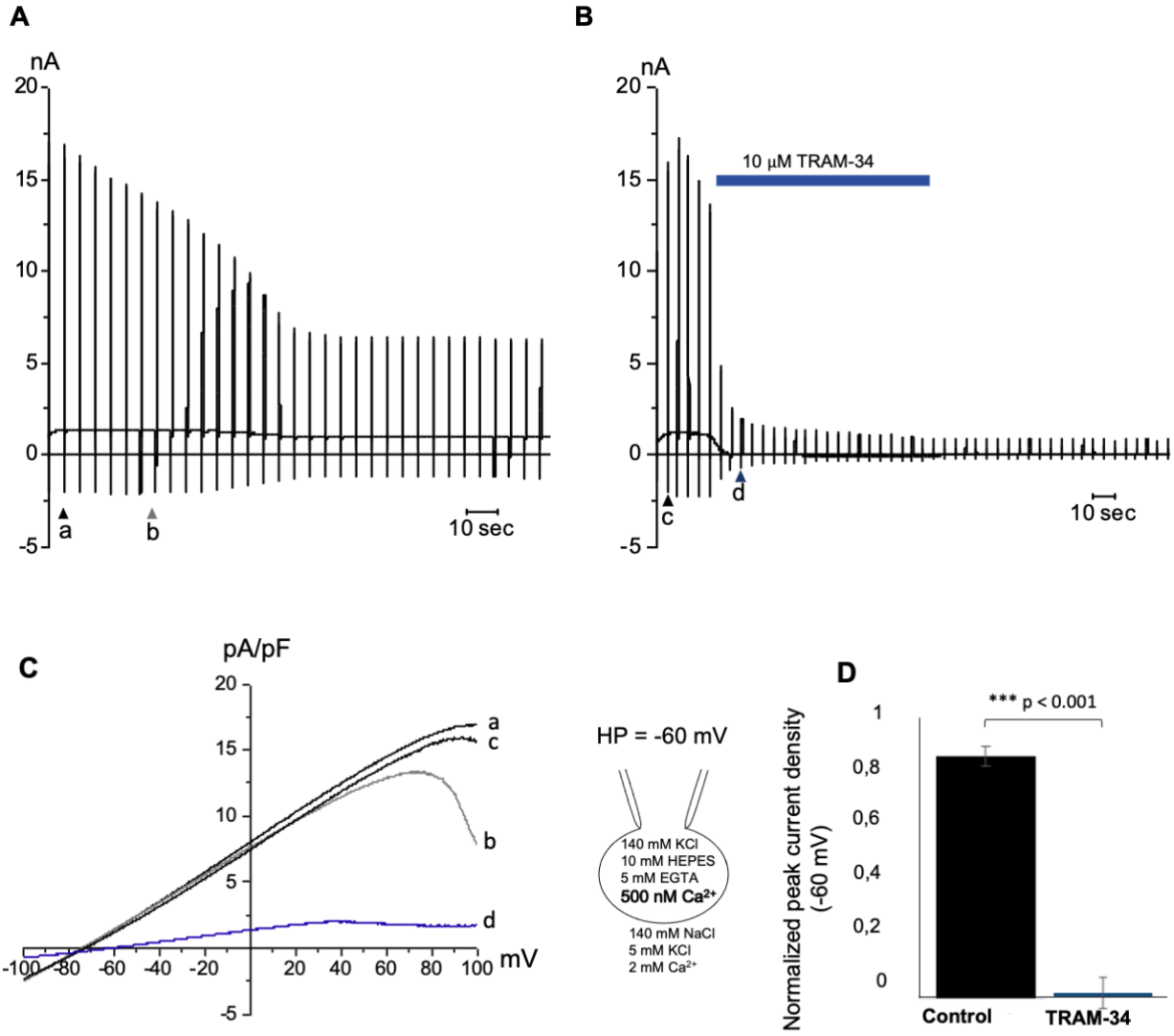
A
nA
20
15
10
5
0
-5
a
b
10 sec
B
nA
10 µM TRAM-34
c
d
10 sec
C
pA/pF
a
c
b
d
-100 -80 -60 -40 -20 20 40 60 80 100 mV
HP = -60 mV
140 mM KCl
10 mM HEPES
5 mM EGTA
500 nM Ca2+
140 mM NaCl
5 mM KCl
2 mM Ca2+
D
*** p < 0.001
Normalized peak current density (-60 mV)
1
0,8
0,6
0,4
0,2
0
Control
TRAM-34

Figure 5. TRAM-34 specifically inhibited the $IK_{Ca}1$ channel

(A) Representative whole-cell current traces of $IK_{Ca}1$ channel activation in response to intracellular 500 nM Ca^{2+} concentration with ramp pulses from -100 mV to +100 mV for 500 msec every 5 sec; holding potential = -60 mV. (n = 13).

(B) Representative whole-cell current traces of $IK_{Ca}1$ channel activation in response to intracellular 500 nM Ca^{2+} concentration and his inhibition by 10 μM TRAM-34 (n = 9).

(C) Current-voltage (IV) curves at the time points indicated by the triangles (n = 13-9).

(D) Normalized peak current density of $IK_{Ca}1$ channel with or without 10 μM TRAM-34. Second time point divided by the first time point. (Means ± SEM (n = 13-9). ***, $p < 0.001$, student t-test).

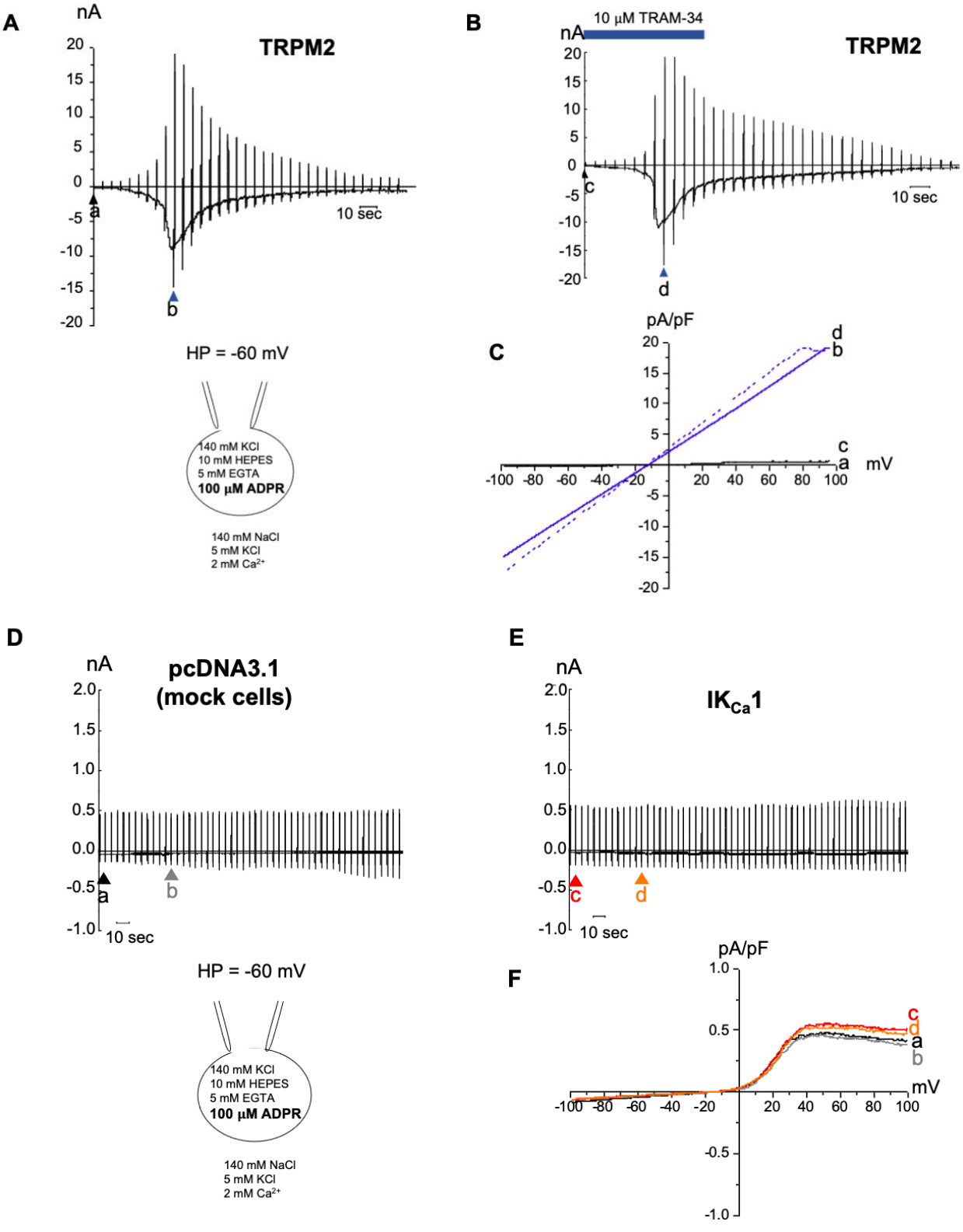
A
nA
TRPM2
20
15
10
5
0
-5
-10
-15
-20
a
b
10 sec
HP = -60 mV
140 mM KCl
10 mM HEPES
5 mM EGTA
100 µM ADPR
140 mM NaCl
5 mM KCl
2 mM Ca2+
B
10 µM TRAM-34
nA
TRPM2
c
d
10 sec
C
pA/pF
d
b
c
a
mV
-100 -80 -60 -40 -20 20 40 60 80 100
D
nA
pcDNA3.1
(mock cells)
2.0
1.5
1.0
0.5
0.0
-0.5
-1.0
a
b
10 sec
HP = -60 mV
140 mM KCl
10 mM HEPES
5 mM EGTA
100 µM ADPR
140 mM NaCl
5 mM KCl
2 mM Ca2+
E
nA
IKCa1
c
d
10 sec
F
pA/pF
1.0
0.5
-0.5
-1.0
c
d
a
b
mV
-100 -80 -60 -40 -20 20 40 60 80 100

Figure 6. The effect of 10 μM TRAM-34 and 100 μM ADPR on $IK_{Ca}1$ and TRPM2 channels

(A) Representative whole-cell current traces of TRPM2 channel activation in response to an intracellular 100 μM concentration of ADPR with ramp pulses from -100 mV to +100 mV for 500 msec every 5 sec; holding potential = -60 mV (n = 15).

(B) TRPM2 current after 10 μM TRAM-34 application (n = 12).

(C) Current-voltage (IV) curves at the time points indicated by the triangles. Normalized peak current density of TRPM2 channel with (28.0 ± 6.8 nA) or without 10 μM TRAM-34 application (31.7 ± 7.4 nA). Data were normalized by dividing the second time point by the first time point.

(D) Representative whole-cell current traces of pcDNA3.1 (mock cells) in 100 μM ADPR intracellular concentration with ramp pulses from -100 mV to +100 mV for 500 msec every 5 sec; holding potential = -60 mV (n = 11).

(E) Representative whole-cell current traces of $IK_{Ca}1$ with 100 μM ADPR intracellular concentration with ramp pulses from -100 mV to +100 mV for 500 msec every 5 sec; holding potential = -60 mV (n = 12).

(F) Current-voltage (IV) curves at the time points indicated by the triangles for a mock cell (pcDNA3.1) (0.8 ± 0.1 nA) and a cell expressing $IK_{Ca}1$ (0.8 ± 0.1 nA) exposed to intracellular ADPR (100 μM). Normalized peak current density of mock cells and $IK_{Ca}1$ channel with application of intracellular ADPR (100 μM). Data were normalized by dividing the second time point by the first time point.

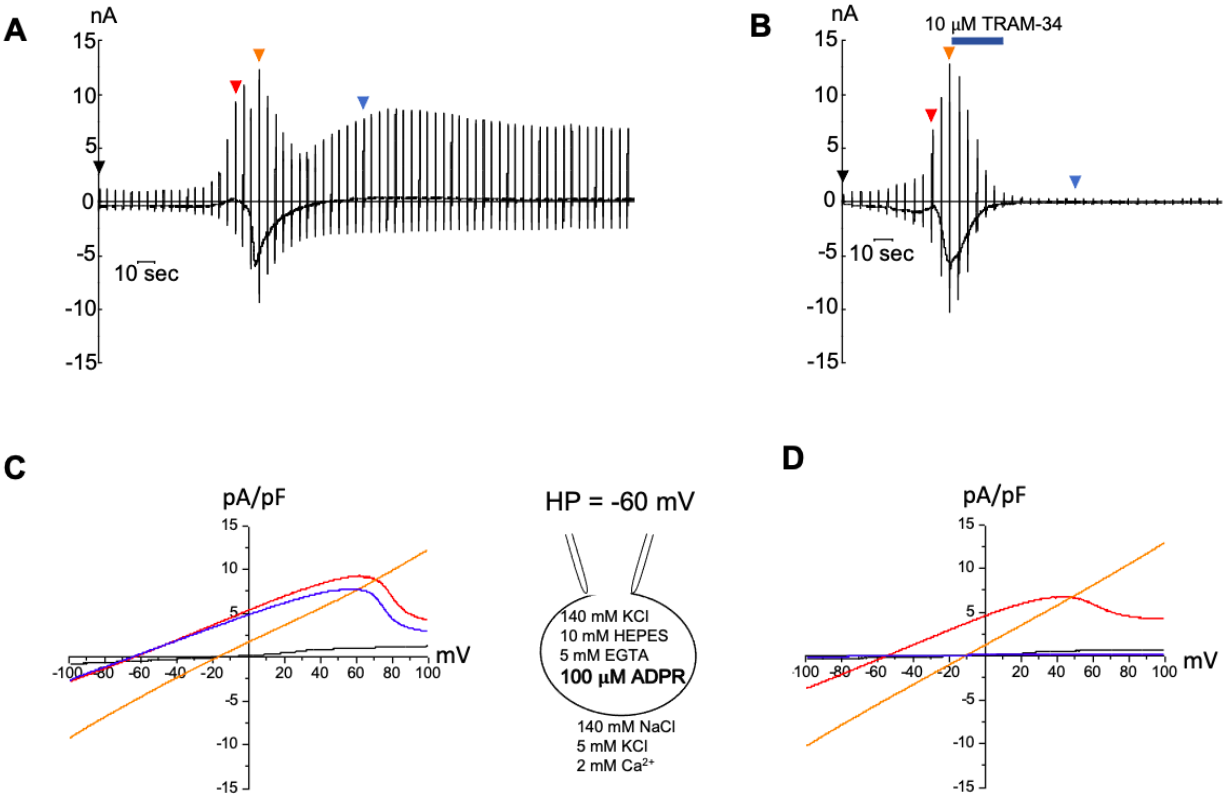

E

E_{rev}	▼	▼	▼	▼
CONTROL	-19.1 ± 2.3 mV	-56.8 ± 2.9 mV	-29.0 ± 4.3 mV	-62.2 ± 3.1 mV
TRAM-34	-13.3 ± 1.0 mV	-50.3 ± 2.0 mV	-18.2 ± 2.1 mV	-25.2 ± 4.6 mV

*** $p < 0.001$

Figure 7. Activation of the $IK_{Ca}1$ channel by Ca^{2+} that entered via ADPR induced-TRPM2 in HEK293T cells

(A-B) Representative whole-cell current traces of HEK293T cells expressing the $IK_{Ca}1$ / TRPM2 channels. TRPM2 was activated with 100 μM intracellular ADPR. Ramp pulses from -100 mV to +100 mV for 500 msec every 5 sec; holding potential = -60 mV. (A) is without 10 μM TRAM-34 (n = 16) and (B) is with 10 μM TRAM-34 (n = 14).

(C-D) Current-voltage (IV) curves at the time points indicated by the triangles on (A) and (B).

(E) Table summarizing the E_{rev} shift throughout the recording for both conditions. CONTROL for non-treated cell, TRAM-34 for 10 μM TRAM-34 treated cells. Means ± SEM (n = 16 - 14). ***, $p < 0.001$ (one-way ANOVA followed by post hoc Bonferroni test for multiple comparison).

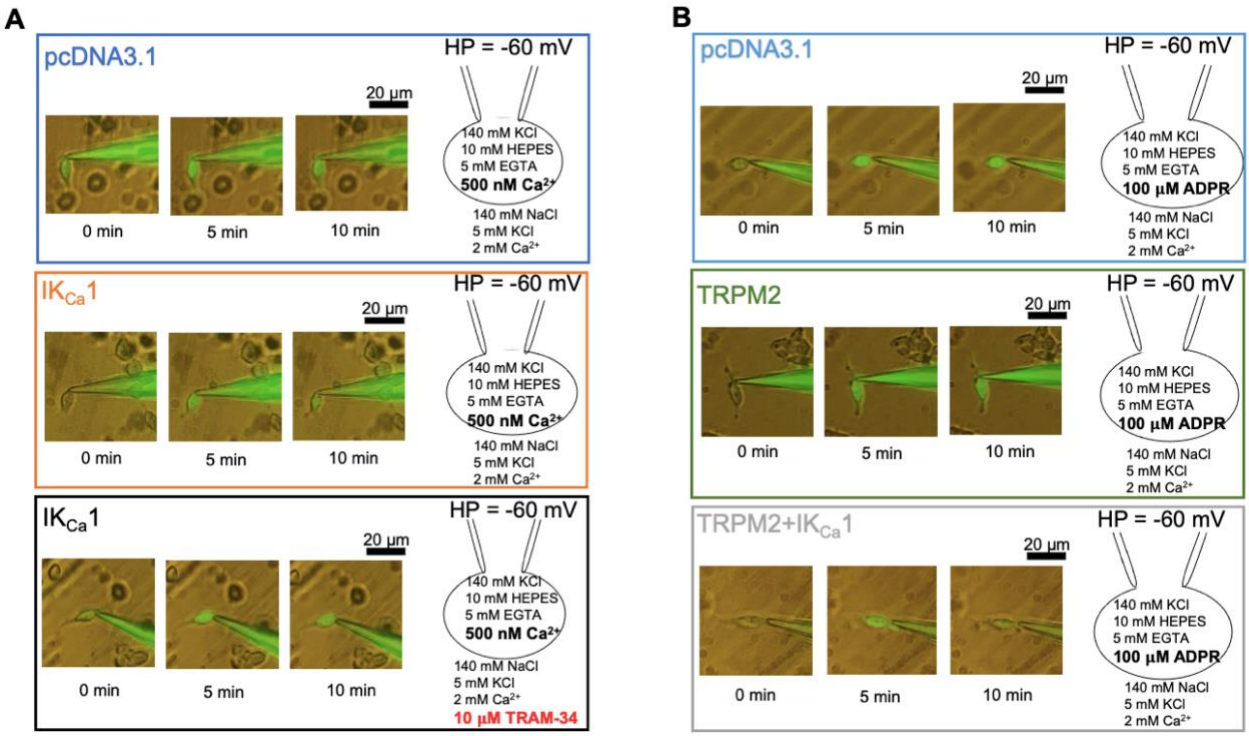

Effect of K^+ efflux on cell volume changes

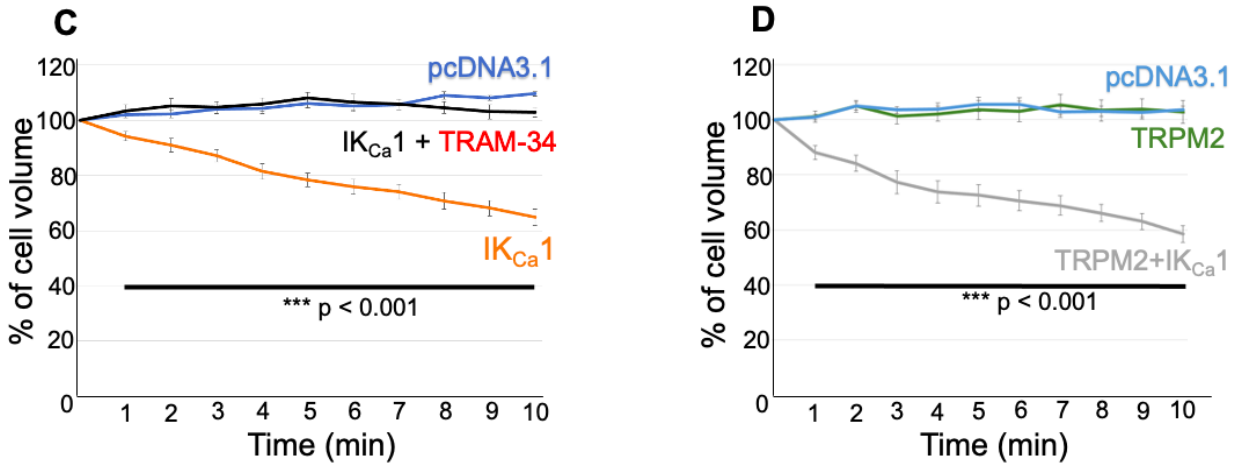

Figure 8. Effect of K^+ flux on volume changes in HEK293T cells

(A-B) Representative cell volume changes in each condition. Blue (n = 12), Orange (n = 14), Black (n = 11), Sky Blue (n = 11), Green (n = 11), Gray (n = 11)

(C) Graph representing the percentage of cell volume throughout the recording for each condition. ***, $p < 0.001$ (one-way ANOVA followed by post hoc Bonferroni test for multiple comparisons).

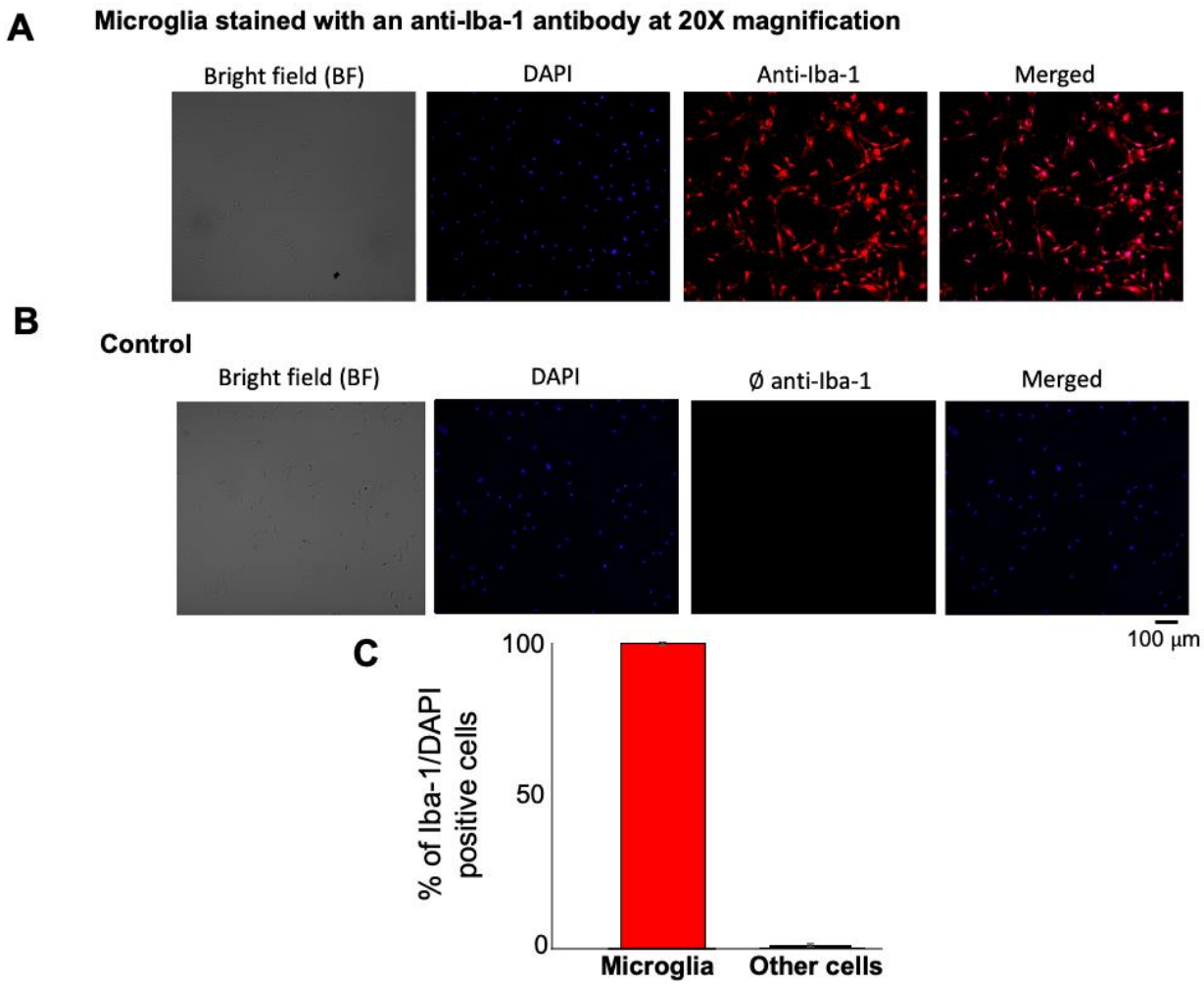
A
Microglia stained with an anti-Iba-1 antibody at 20X magnification
Bright field (BF)
DAPI
Anti-Iba-1
Merged
B
Control
Bright field (BF)
DAPI
Ø anti-Iba-1
Merged
100 µm
C
% of Iba-1/DAPI positive cells
100
50
0
Microglia
Other cells

Figure 9. Immunofluorescence staining of Iba-1 in microglia to determine the purity of culture

(A) Representative image of microglia stained with anti-Iba-1 antibody (from left to right: Bright field, DAPI, anti-Iba-1, Merged).

(B) Control image of microglia without anti-Iba1 antibody staining (from left to right: Bright field, DAPI, anti-Iba-1, Merged).

(C) Percentage of Iba-1/DAPI positive cells showing the purity of microglia after shaking from glial culture. We counted the cells labeled with anti-Iba-1/DAPI and cells labeled only with DAPI in order to determine the percentage of purity. The results suggested that approximately 98% of the cells are microglia.

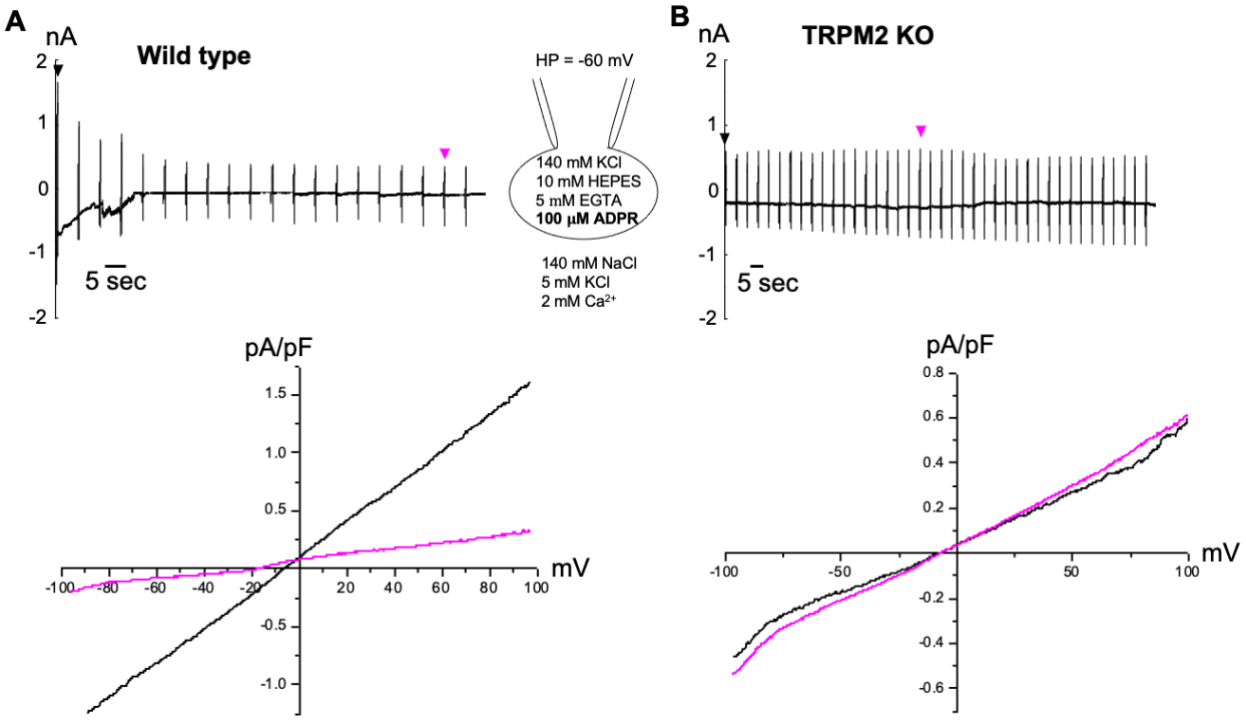

C

	▼	▼
WT	-4.9 ± 1.0 mV	-12.1 ± 2.1 mV
TRPM2 KO	-8.8 ± 1.9 mV	-13.2 ± 2.5 mV

Figure 10. Ca^{2+} influx through TRPM2 activation with 100 μM ADPR was insufficient to activate the $IK_{Ca}1$ channel

Representative whole-cell current traces of WT and TRPM2 KO mouse primary microglia.

(A) WT microglia were patched with KCl pipette solution containing 100 μM ADPR. TRPM2 was activated with intracellular 100 μM ADPR. Ramp pulses from -100 mV to +100 mV for 500 msec every 5 sec; holding potential= -60 mV. Means ± SEM (n = 17).

(B) TRPM2 KO microglia were patched with KCl pipette solution containing 100 μM ADPR. Ramp pulses from -100 mV to +100 mV for 500 msec every 5 sec; holding potential = -60 mV. Means ± SEM (n = 6).

(C) Table summarizing the E_{rev} throughout the recording for A and B conditions. Means ± SEM (n = 17 - 6)

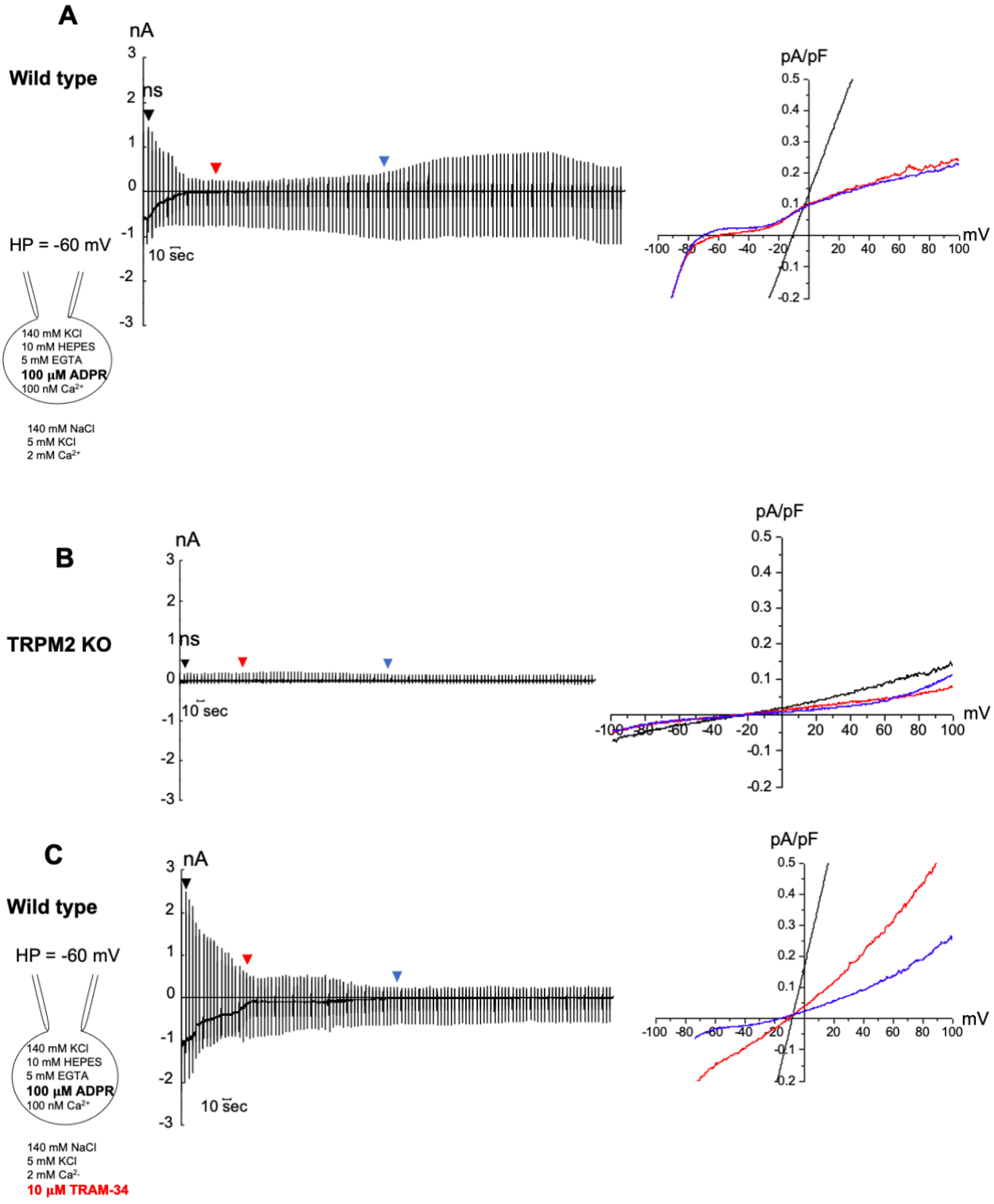
A
Wild type
nA
ns
10 sec
HP = -60 mV
140 mM KCl
10 mM HEPES
5 mM EGTA
100 µM ADPR
100 nM Ca2+
140 mM NaCl
5 mM KCl
2 mM Ca2+
pA/pF
mV
B
TRPM2 KO
nA
ns
10 sec
pA/pF
mV
C
Wild type
nA
HP = -60 mV
140 mM KCl
10 mM HEPES
5 mM EGTA
100 µM ADPR
100 nM Ca2+
140 mM NaCl
5 mM KCl
2 mM Ca2+
10 µM TRAM-34
10 sec
pA/pF
mV

D

	▼	▼	▼
WT	-17.2 ± 2.3 mV	-56.1 ± 2.2 mV	-48.3 ± 3.9 mV
TRPM2 KO	-13.3 ± 2.1 mV	-12.2 ± 2.2 mV *** p < 0.001	-9.2 ± 2.2 mV *** p < 0.001
WT-TRAM-34	-6.5 ± 1.2 mV ** p < 0.01	-13.4 ± 1.9 mV *** p < 0.001	-16.1 ± 2.0 mV *** p < 0.001

E

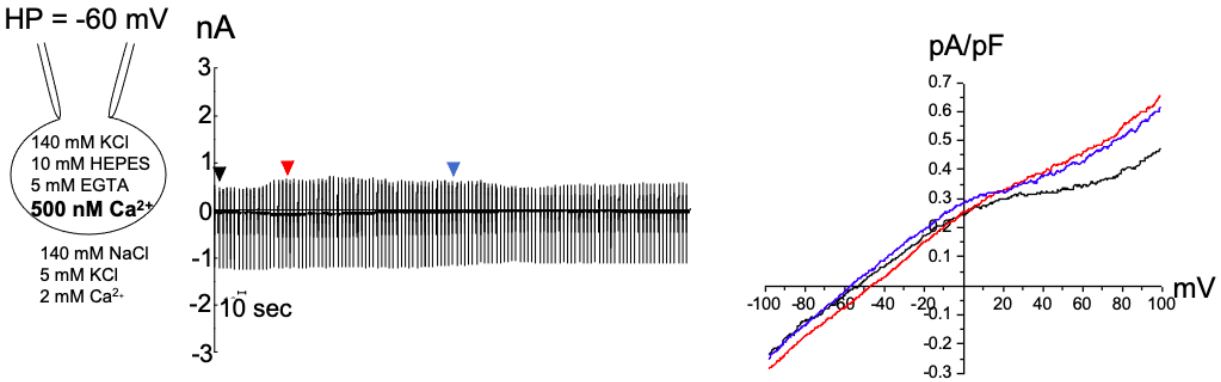

TRPM2 KO

F

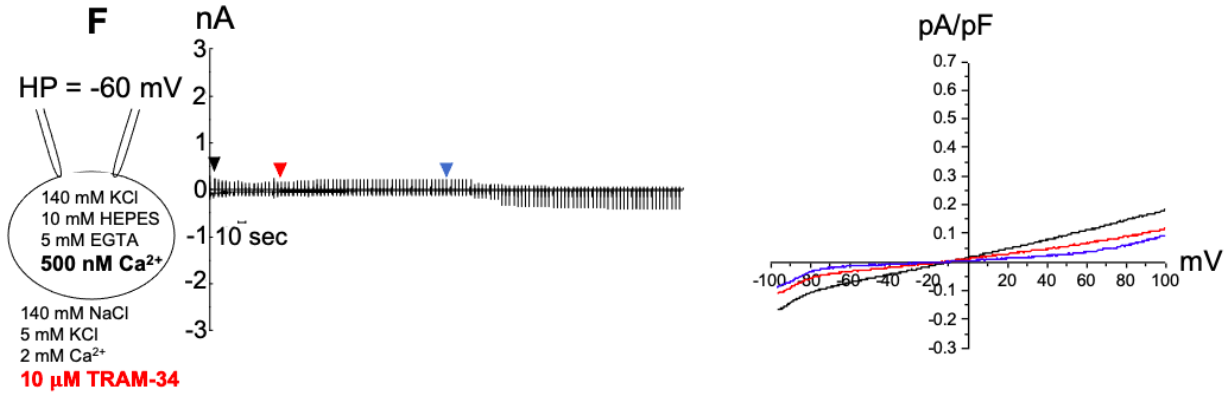

G

	▼	▼	▼
TRPM2 KO	-66.4 ± 3.1 mV	-62.6 ± 4.6 mV	-59.7 ± 5.9 mV
TRPM2 KO-TRAM-34	-16.3 ± 1.7 mV *** p < 0.001	-19.5 ± 2.3 mV *** p < 0.001	-24.6 ± 2.9 mV *** p < 0.001

Figure 11. $IK_{Ca}1$ channel activation through Ca^{2+} entering by ADPR induced-TRPM2 in mouse primary microglia

Representative whole-cell current traces of WT and TRPM2 KO mouse primary microglia.

(A) WT microglia were patched with a KCl pipette solution containing 100 μM ADPR. TRPM2 was activated with intracellular 100 μM ADPR and the induce E_{rev} shift towards -60 mV shows the activation of the $IK_{Ca}1$ channel. Ramp pulses from -100 mV to +100 mV for 500 msec every 5 sec; holding potential = -60 mV.

(B) TRPM2 KO microglia were patched with a KCl pipette solution containing 100 μM ADPR. Because TRPM2 was absent, Ca^{2+} could not enter through this channel and the $IK_{Ca}1$ channel was not activated. The E_{rev} remained around -13 mV.

(C) WT microglia were patched with a KCl pipette solution containing 100 μM ADPR. TRPM2 was activated with intracellular ADPR at 100 μM. However, activation of the $IK_{Ca}1$ channel did not occur when cells were treated with 10 μM TRAM-34. The E_{rev} shift was not observed.

(D) Table summarizing the E_{rev} shift throughout the recording for A, B and C conditions. Means ± SEM (n = 11 - 12). ***, $p < 0.001$ (one-way ANOVA followed by post hoc Bonferroni test for multiple comparison).

(E) TRPM2 KO microglia were patched with a KCl pipette solution containing 500 nM Ca^{2+} in order to directly trigger the $IK_{Ca}1$ channel. The E_{rev} were around -66 mV and remained around this value.

(F) TRPM2 KO microglia were patched with a KCl pipette solution containing 500 nM Ca^{2+} in order to directly trigger the $IK_{Ca}1$ channel. However, activation of the $IK_{Ca}1$ channel did not occur when cells were treated with 10 μM TRAM-34. The E_{rev} values were around -16 mV and remained fairly constant.

(G) Table summarizes the E_{rev} values throughout the recording for E and F conditions. Means ± SEM (n = 11 - 12). **, $p < 0.01$; ***, $p < 0.001$ (one-way ANOVA followed by post hoc

Bonferroni test for multiple comparison).

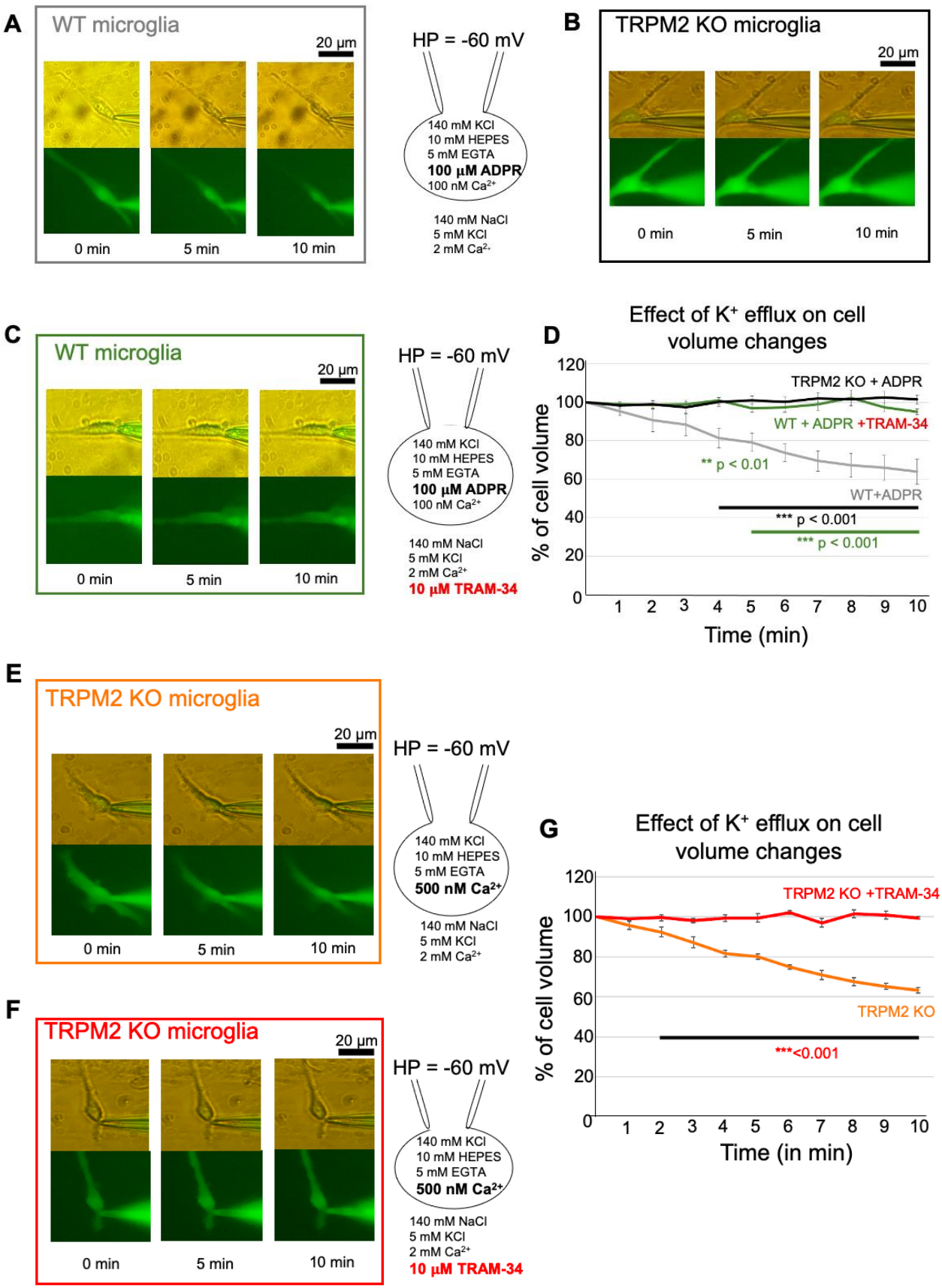
A
WT microglia
20 µm
0 min
5 min
10 min
HP = -60 mV
140 mM KCl
10 mM HEPES
5 mM EGTA
100 µM ADPR
100 nM Ca2+
140 mM NaCl
5 mM KCl
2 mM Ca2+
B
TRPM2 KO microglia
20 µm
0 min
5 min
10 min
C
WT microglia
20 µm
0 min
5 min
10 min
HP = -60 mV
140 mM KCl
10 mM HEPES
5 mM EGTA
100 µM ADPR
100 nM Ca2+
140 mM NaCl
5 mM KCl
2 mM Ca2+
10 µM TRAM-34
D
Effect of K+ efflux on cell volume changes
% of cell volume
Time (min)
TRPM2 KO + ADPR
WT + ADPR +TRAM-34
** p < 0.01
WT+ADPR
*** p < 0.001
*** p < 0.001
E
TRPM2 KO microglia
20 µm
0 min
5 min
10 min
HP = -60 mV
140 mM KCl
10 mM HEPES
5 mM EGTA
500 nM Ca2+
140 mM NaCl
5 mM KCl
2 mM Ca2+
F
TRPM2 KO microglia
20 µm
0 min
5 min
10 min
HP = -60 mV
140 mM KCl
10 mM HEPES
5 mM EGTA
500 nM Ca2+
140 mM NaCl
5 mM KCl
2 mM Ca2+
10 µM TRAM-34
G
Effect of K+ efflux on cell volume changes
% of cell volume
Time (in min)
TRPM2 KO +TRAM-34
TRPM2 KO
***<0.001

Figure 12. Effect of K^+ flux on volume changes in mouse primary microglia

(A-F) Representative cell volume changes in each condition. WT-ADPR represented by the gray line (n = 5), TRPM2 KO-ADPR represented by the black line (n = 5), WT-ADPR + TRAM-34 represented by the green line (n = 6), TRPM2 KO-500 nM Ca^{2+} represented by the orange line (n = 6), TRPM2 KO + 500 nM Ca^{2+}-TRAM-34 represented by the red line (n = 8). (D and G) Graphs representing the percentage of cell volume throughout the recording for each condition. **, $p < 0.01$, ***, $p < 0.001$ (one-way ANOVA followed by post hoc Bonferroni test for multiple comparison).

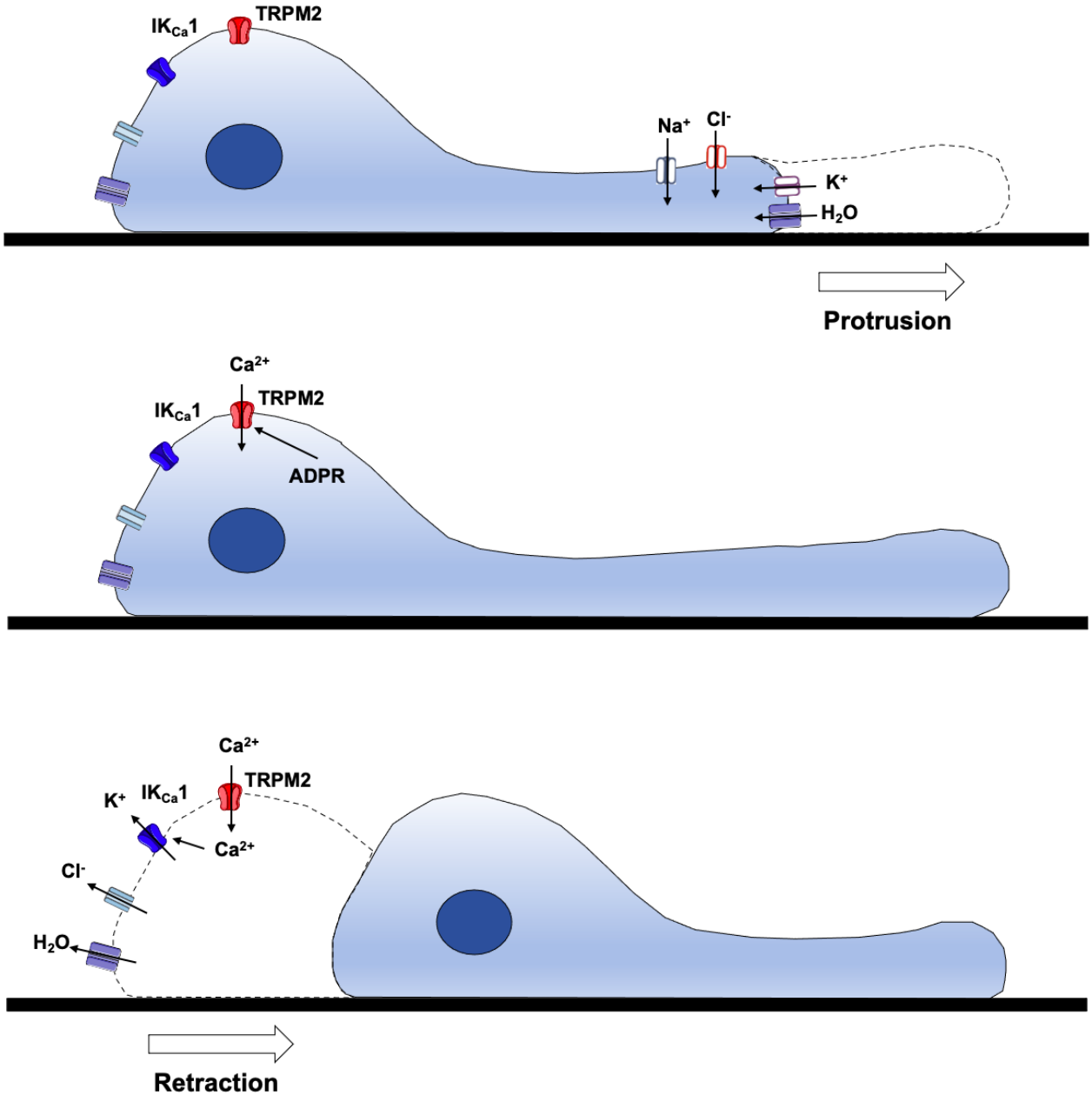
IK$_{Ca}$1
TRPM2
Na$^+$
Cl$^-$
K$^+$
H$_2$O
Protrusion
Ca^{2+}
IK$_{Ca}$1
TRPM2
ADPR
Ca^{2+}
K$^+$
IK$_{Ca}$1
TRPM2
Ca^{2+}
Cl$^-$
H$_2$O
Retraction

Figure 13. Schematic representation of cell volume changes during cell migration

Model summarizing the role of TRPM2 and $IK_{Ca}1$ channels in controlling microglial migration. TRPM2 activation through ADPR induces Ca^{2+} influx. The Ca^{2+} binds to the N iii CaM domain of $IK_{Ca}1$ and pulls the homotetramer subunit, leading to the opening of $IK_{Ca}1$ channels. Activation of $IK_{Ca}1$ induces K^+ efflux. K^+ efflux is accompanied by Cl^- efflux and H_2O loss leading to a shrinkage of the cell at the rear portion of the microglial cell.

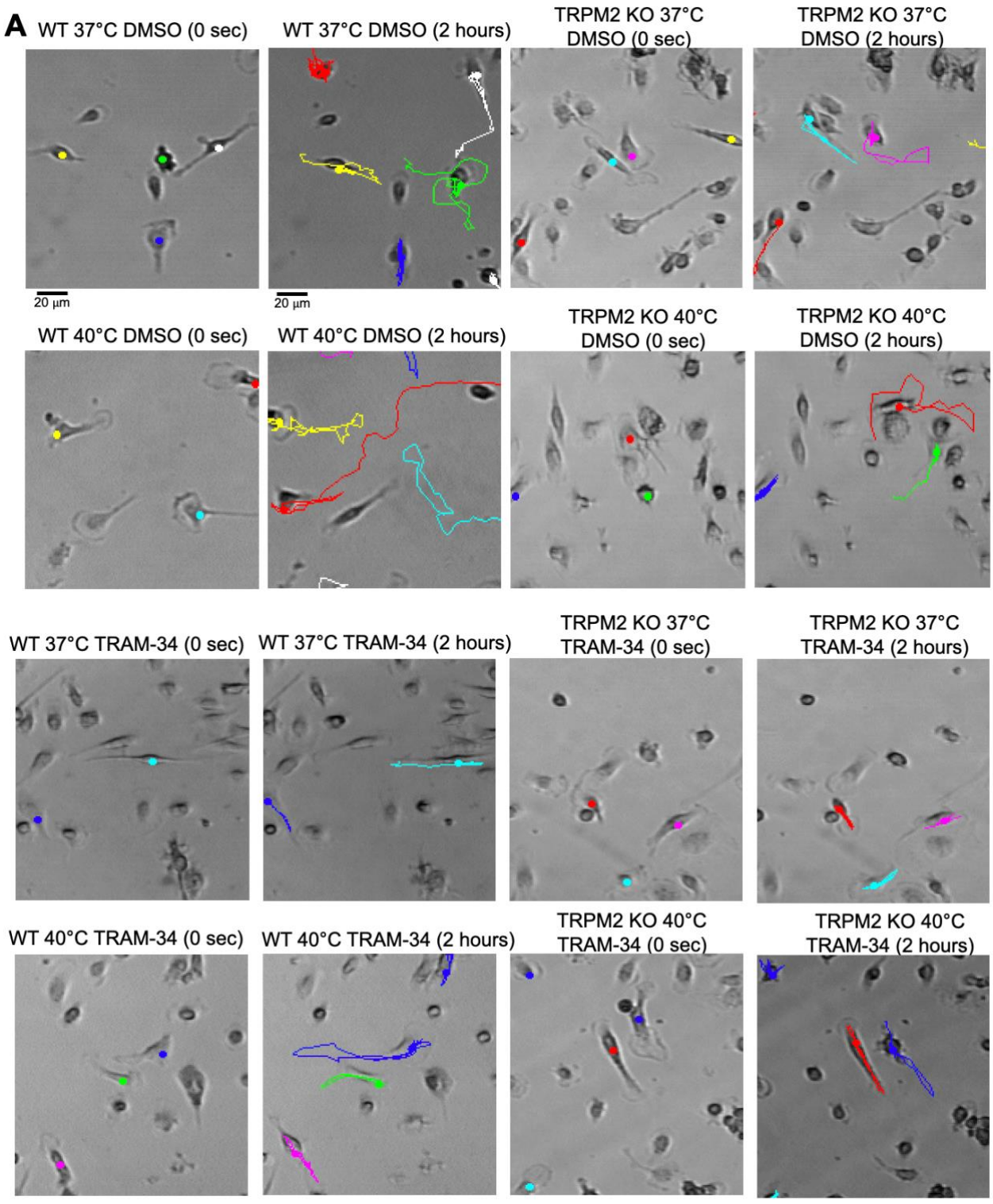
A
WT 37°C DMSO (0 sec)
WT 37°C DMSO (2 hours)
TRPM2 KO 37°C DMSO (0 sec)
TRPM2 KO 37°C DMSO (2 hours)
20 µm
20 µm
WT 40°C DMSO (0 sec)
WT 40°C DMSO (2 hours)
TRPM2 KO 40°C DMSO (0 sec)
TRPM2 KO 40°C DMSO (2 hours)
WT 37°C TRAM-34 (0 sec)
WT 37°C TRAM-34 (2 hours)
TRPM2 KO 37°C TRAM-34 (0 sec)
TRPM2 KO 37°C TRAM-34 (2 hours)
WT 40°C TRAM-34 (0 sec)
WT 40°C TRAM-34 (2 hours)
TRPM2 KO 40°C TRAM-34 (0 sec)
TRPM2 KO 40°C TRAM-34 (2 hours)

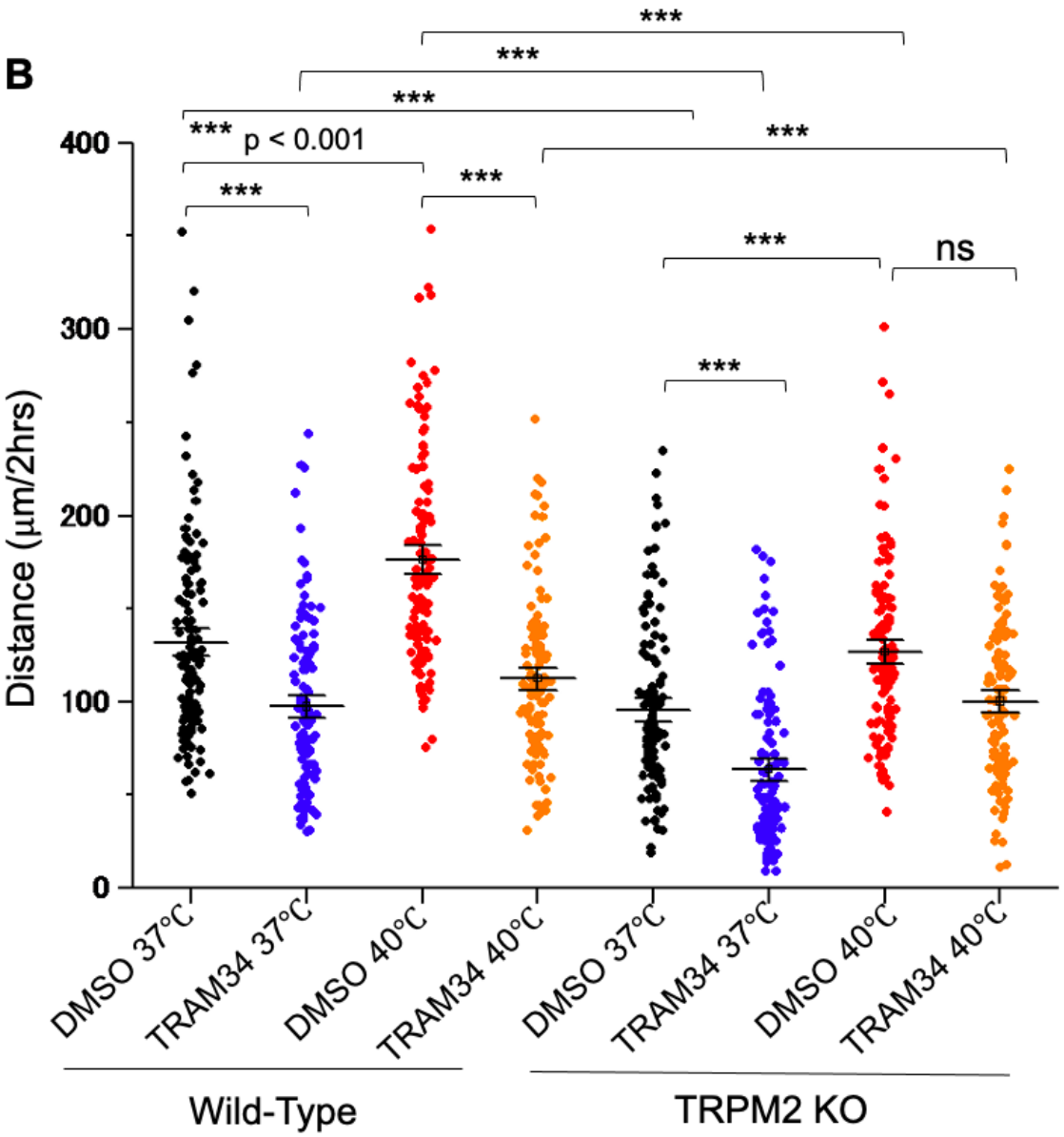
B
***
***
***
*** p < 0.001
***
***
***
***
ns
***
400
300
200
100
0
Distance (µm/2hrs)
DMSO 37°C
TRAM34 37°C
DMSO 40°C
TRAM34 40°C
DMSO 37°C
TRAM34 37°C
DMSO 40°C
TRAM34 40°C
Wild-Type
TRPM2 KO

Figure 14. Mouse primary microglia exhibit TRPM2 / $IK_{Ca}1$-dependent motility *in vitro*

(A) Representative images of all conditions at 37°C and 40°C from time-lapse imaging. Images taken at time 0 and 2 h are shown on the left and right respectively. Filled colored circles indicate *x,y* coordinates of a representative target and colored lines indicate trajectory. The trajectories were superimposed on the images using ImageJ Manual tracking plugin. (Scale bar represents 50 μm).

(B) Average distances of migrating microglia isolated from WT and TRPM2 KO mice exposed to 37°C and 40°C in the presence or absence of 10 μM TRAM-34 (for each condition n = 120 cells). Horizontal lines indicate means ± SEM. ***, $p < 0.001$ (non-parametric Wilcoxon/Kruskal-Wallis test followed by post hoc Steel-Dwass method comparison all pairs).

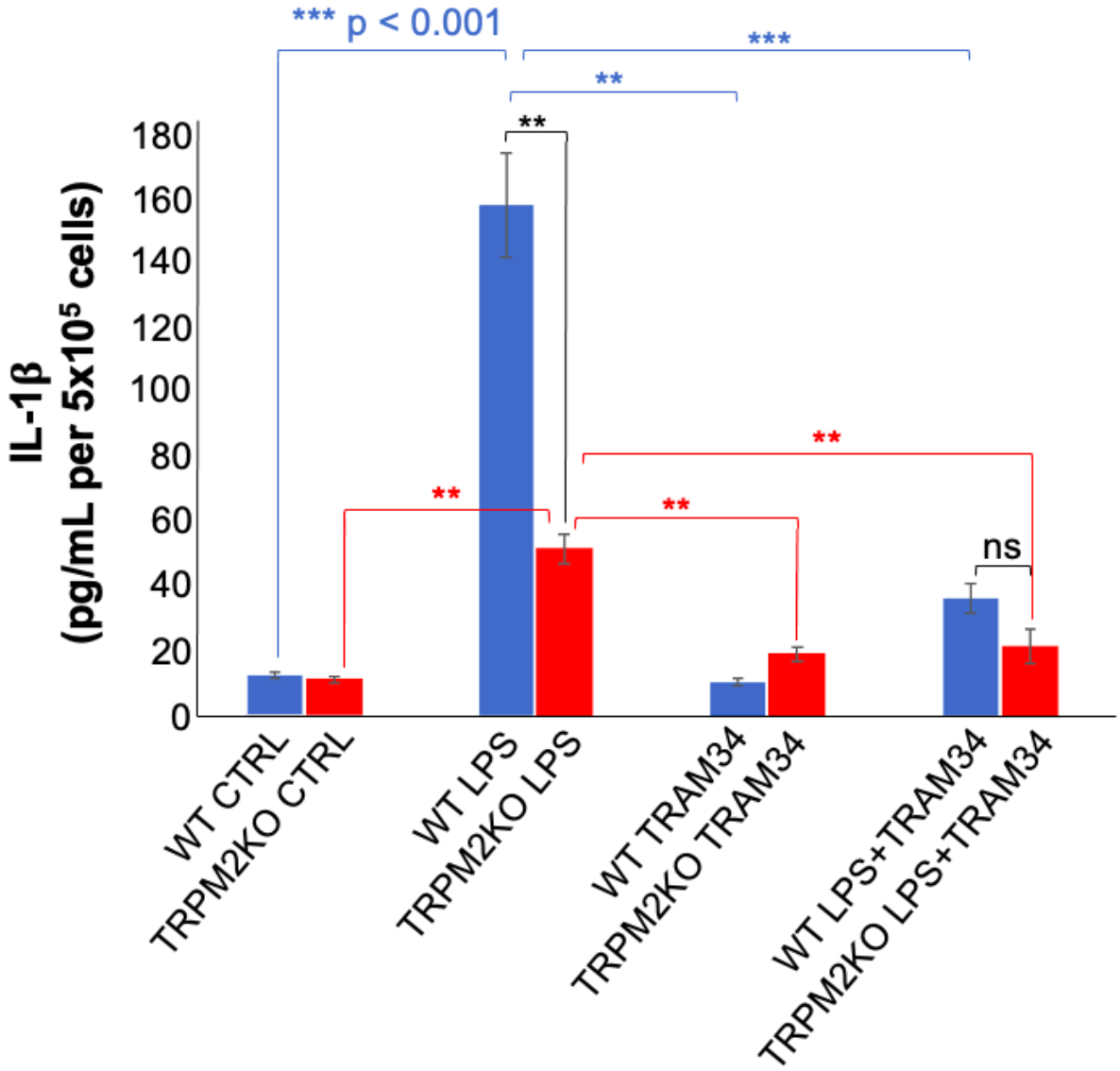
*** p < 0.001
***
**
**
**
**
**
ns
IL-1β
(pg/mL per 5x10⁵ cells)
180
160
140
120
100
80
60
40
20
0
WT CTRL
TRPM2KO CTRL
WT LPS
TRPM2KO LPS
WT TRAM34
TRPM2KO TRAM34
WT LPS+TRAM34
TRPM2KO LPS+TRAM34

Figure 15. Cytokine production by mouse primary microglia through the TRPM2 / $IK_{Ca}1$ network

Plot shows the concentration of IL-1β released by 5 x 10^5 WT and TRPM2 KO mouse primary microglia after 48 h incubation with 100 ng/mL LPS at 37°C. ***, $p < 0.001$ (non-parametric Wilcoxon/Kruskal-Wallis test followed by post hoc Steel-Dwass method comparison all pairs).

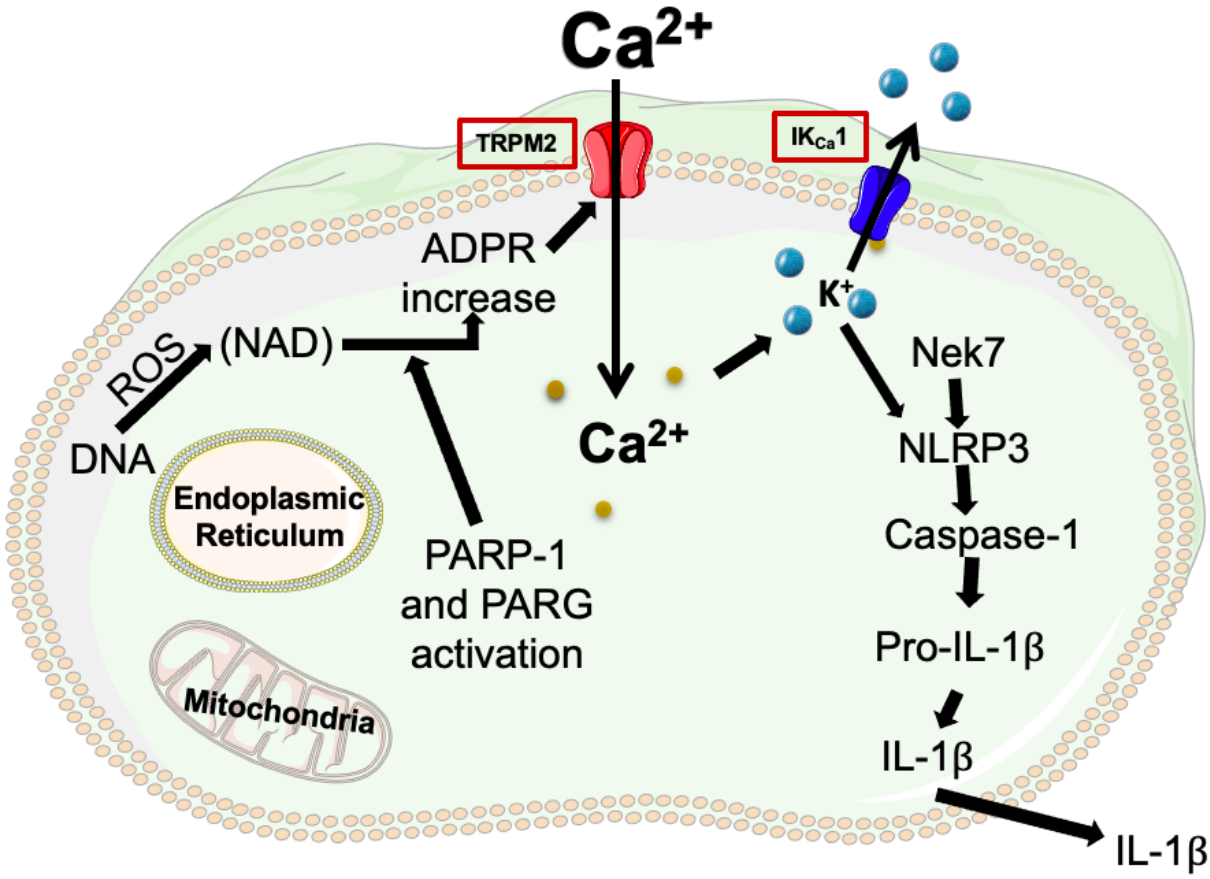
Ca2+
TRPM2
IKCa1
ADPR
increase
K+
ROS
(NAD)
Nek7
DNA
Ca2+
NLRP3
Endoplasmic
Reticulum
Caspase-1
PARP-1
and PARG
activation
Pro-IL-1β
Mitochondria
IL-1β
IL-1β

Figure 16. A proposed pathway for cytokine production by primary mouse microglia through the TRPM2 / $IK_{Ca}1$ network

Schematic representation of cytokine production by mouse primary microglia through $IK_{Ca}1$-induced K^+ efflux. NLRP3 senses the K^+ efflux. NEK7 shown to directly bind its catalytic domain to the LRR domain of NLRP3 and regulates its oligomerization and activation. The positive regulation of NLRP3 leads to the activation of caspase-1 and maturation of IL-1β.

A **Nernst equation for equilibrium potential**

For $IK_{Ca}1$:

KCl pipette solution

$$E_{rev} = \frac{RT}{F} \ln \frac{[K^+]_o}{[K^+]_i}$$

$$E_{rev} = \frac{8.314*(25+273.15)}{96485} \ln \frac{5}{140}$$

$$E_{rev} = \frac{2478.8191}{96485} \ln \frac{5}{140}$$

$$E_{rev} = 0.0256912 \ln \frac{5}{140} \approx -0.0856 \text{ V}$$

$$\approx -86 \text{ mV}$$

HP = -60 mV

140 mM NaCl
5 mM KCl
2 mM Ca^{2+}

B **Goldman-Hodgkin-Katz equation for equilibrium potential**

For TRPM2:

KCl pipette solution

$$E_{rev} = \frac{RT}{F} \ln \frac{P_{K+}[K^+]_o + P_{K+}[Ca^{2+}]_o + P_{K+}[Na^+]_o}{P_{K+}[K^+]_i + P_{K+}[Ca^{2+}]_i + P_{K+}[Na^+]_i}$$

$$E_{rev} = \frac{8.314*(25+273.15)}{96485} \ln \frac{(1.1 \times 5) + (0.9 \times 2) + (1.1 \times 140)}{(1.1 \times 140) + (0.9 \times 0) + (1.1 \times 0)}$$

$$E_{rev} = \frac{2478.8191}{96485} \ln \frac{161.3}{154}$$

$$E_{rev} = 0.0256912 \ln \frac{161.3}{154} \approx 0.001189 \text{ V}$$

$$\approx 1{,}18 \text{ mV}$$

HP = -60 mV

140 mM NaCl
5 mM KCl
2 mM Ca^{2+}

Equations. Nernst equation for $IK_{Ca}1$ equilibrium potential and Goldman-Hodgkin-Katz equation for TRPM2 equilibrium potential.

(A) Nernst equation for $IK_{Ca}1$ ion channel in order to determine the E_{rev}. R (gas constant = 8.3145 $J.mol^{-1}.K^{-1}$), T (absolute temperature = T(C°) + 273.15 K), F (Faraday constant = 98485 C. mol^{-1}).

(B) Goldman-Hodgkin-Katz equation for TRPM2 ion channel in order to determine the E_{rev}. R (gas constant = 8.3145 $J.mol^{-1}.K^{-1}$), T (absolute temperature = T(C°) + 273.15 K), F (Faraday constant = 98485 C. mol^{-1}), P_{ion} (relative permeability). For relative permeability (Turlova, E. et al., 2018)

6. Abbreviations

Ca^{2+}, Calcium

K+, Potassium

Na^{+}, Sodium

ER, Endoplamic Reticulum

TMD, Transmembrane domain

STIM1, Stromal interaction molecule 1

NAD^{+}, Nicotinamide Adenine Dinucleotide

ADPR, Adenosine diphosphate ribose

cADPR, cyclic Adenosine diphosphate ribose

MHD, Homologous domain

NUDT9-H, Nucleoside diphosphate-linked moiety X-type motif 9 domain

AMP, Adenosine diphosphate

PKA, Protein kinase A

AMPK, AMP-activated protein kinase

PI3P, phosphatidylinositol 3-phosphate

TRAM-34, 1-[(2-Chlorophenyl)diphenylmethyl]-1H-pyrazole

CaM, Calmodulin

H_2O_2, Hydrogen peroxide

HEK293T, Human embryonic kidney 293T

TRP, Transient receptor potential

TRPM2, Transient receptor potential melastatin type 2

$IK_{Ca}1$, intermediate calcium-activated-potassium channels 1

IL-1β, Interleukin-1ß

NAADP, nicotinic acid adenine dinucleotide phosphate

ROS, Reactive oxygen species

PARP, Poly-ADPR polymerase

PARG, Poly-ADPR glycohydrolase

ROS, Reactive oxygen species

CNS, Central Nervous System

AD, Alzheimer’s disease

PD, Parkinson’s disease

MS, Multiple Sclerosis

ALS, Amyotrophic lateral sclerosis

WT, Wild-Type

Co-IP, Co-immunoprecipitation

WB, Western Blot

HA, Hemagglutinin

DTT, 1.4-Dithiothreitol

TBS, Tris buffered solution

TBST, Tris buffered solution Tween

RT, Room Temperature

Iba-1, Ionized calcium-binding adapter molecule 1

ERK, Extracellular signal-regulated kinase

GEF-H1, Guanine Nucleotide Exchange Factor

NLRP3, NLR family pyrin domain containing 3

NEK7, NIMA-related kinase

LRR, Leucine-rich repeat proteins

7. Acknowledgement

I would like to thank Prof. M. Tominaga for leading me to the physiological sciences and also for his continuous encouragement and helpful advice throughout this study. I also would like to thank Prof. S. Derouiche, Prof. M. Kashio and Dr. K. Maruyama for advice in the execution of this study. I would also like to thank all of the laboratory members for their input and daily support. Finally, I also like to thank my father, mother, sister, brother and fiancee for their encouragement throughout these past 3 years in Japan.

This study was supported by the Ministry of Education, Culture, Sport, Science and Technology of Japan scholarships for 3 years.

8. References

1. ALIM, I., TEVES, L., LI, R., MORI, Y., AND TYMIANSKI, M., Modulation of NMDAR subunit expression by TRPM2 channels regulates neuronal vulnerability to ischemic cell death. J *Neurosci,* **2013** Oct 30;33(44):17264-77. doi: 10.1523/JNEUROSCI.1729-13.2013.

2. BAI, J.Z., AND LIPSKI, J., Differential expression of TPRM2 and TRPV4 channels ant their potential role in oxidative stress-induced cell death in organotypic hippocampal culture. *Neurotoxicology,* **2010** Mar;31(2):204-14. doi: 10.1016/j.neuro.2020.01.001.

3. BOUHY, D., GHASEMLOU, N., LIVELY, S., REDENSEK, A., RATHORE, K.I., SCHLICHTER, L.C., AND DAVID, S., Inhibition of the Ca^{2+}-dependent K^+ channel, KCNN4/KCa3.1, improves tissue protection and locomotor recovery after spinal cord injury. *J Neurosci,* **2011** Nov 9;31(45):16298-308. doi: 10.1523/JNEUROSCI.0047-11.2011.

4. BRINI, M., CALI, T., OTTOLINI, D., AND CARAFOLI, E., Intracellular calcium homeostasis and signaling. *Met Ions Life Sci,* **2013**; 12:119-68. doi: 10.1007/978-94-007-5561-1_5.

5. BROWN, B.M., LIU, G., PRESSLEY, B., AND WULFF, H., KCa3.1 Channel Modulators as potential Therapeutic Compounds for Glioblastoma. *Curr Neuropharmacol,* **2018**; 16(5):618-626. doi: 10.2174/1570159X15666170630164226.

6. BROWN, B.M., SHIM, H., CHRISTOPHERSEN, P., AND WULFF, H., Pharmacology of Small- and Intermediate-Conductance Calcium-Activated Potassium Channels. *Annu Rev Pharmacol Toxicol,* **2020** Jan 6;60:219-240. doi: 10.1146/annurev-pharmtox-010919-023420. Epub 2019 Jul 23.

7. CARAFOLI, E., AND KREBS, J., Why Calcium? How Calcium Became the best Communicator. *J Biol Chem,* **2016** Sep 30;291(40):20849-20857. doi: 10.1074/jbc.R116.735894.

8. CHEN, X., LIU, G., YUAN, Y., WU, G., WANG, S., AND YUAN, L., NEK7 interact with NLRP3 to modulate the pyroptosis in inflammatory bowel disease via NF-κB signaling. *Cell Death,* **2019** Dec 2;10(12):906., doi: 10.1038/s41419-019-2157-1.

9. CHEN, Y., MENG, J., BI, F., LI, H., CHANG, C., CHEN, J., AND LIU, W., NEK7 Regulated NLRP3 Inflammasome Activation and Neuroinflammation Post-traumatic Brain Injury. *Front*

Mol Neurosci, **2019** Oct 15;12:247., doi: 10.3389/fnmol.2019.00247.
10. CHEUNG, J.Y., AND MILLER, B.A., Transient Receptor potential-Melastatin Channel Familly Member 2: Friend or For. *Trans Am Clin Climatol Assoc,* **2017** 2017;128:308-329

11. CLAPHAM, D.E., Calcium Signaling. *Cell,* **2007** Dec14; Vol 131, issus 6, p1047-1058., doi: 10.1016/j.cell2007.11.028

12. COJOCARU, A., BURADA, E., BALSEANU, A.T., DEFTU, A.F., CATALIN, B., POPA-WAGNER, A., AND OSIAC, E., Roles of Microglia Ion Channel in Neurodegenerative Diseases. *J Clin Med.,* **2021** Mar 17;10(6):1239. doi: 10.3390/jcm10061239.

13. DE BIASE, L.M., SCHUELBEL, K.E., FUSFELD, Z.H., JAIR, K., HAWES, I.A., CIMBRO, R., ZHANG, H.Y., LIU, Q.R., SHEN, H., XI, Z.X., GOLDMAN, D., AND BONCI, A., Local Cues Establish and Maintain Region-Specific Phenotypes of Basal Ganglia Microglia. *Neuron,* **2017** Jul 19;95(2):341-356.e6. doi: 10.1016/j.neuron.2017.06.020.

14. DI, A., KIYA, T., GONG, H., GAO, X., AND MALIK, A.B., Role of the phagosomal redox-sensitive TRP TRPM2 in regulation bactericidal activity of macrophages. *J Cell Sci,* **2017** Feb 15;130(4):735-744. doi: 10.1242/jcs.196014.

15. DOERING, L.C., Protocols for Neural Cell Culture (Humana, New York, **2010**), p.1. *Springer Protocols Handbooks.*

16. DUCHARME, G., NEWELL, E.W., PINTO, C., AND SCHLICHTER, L.C., Small-conductance Cl-channels contribute to volume regulation and phagocytosis in microglia. *Eur J Neurosci,* **2007** Oct;26(8):2119-30 15. doi: 10.1111/j.1460-9568.2007.05802.x.

17. EISFELD, J., AND LUCKHOFF, A., TRPM2. *Handb Exp Pharmacol,* **2007**, (179): 237-52. doi: 10.1007/978-3-540-34891-7_14.

18. FERREIRA, R., AND SCHLICHTER, L.C., Selective activation of KCa3.1 and CRAC channels by P2Y2 receptors promotes Ca(2+) signaling, store refilling and migration of rat microglia cells. *PLoS One,* **2013**, Apr 19;8(4):e62345. doi: 10.1371/journal.pone.0062345.

19. FONFRIA, E., MARSHALL, I.C.B., BENHAM, C.D., BOYFIELD, I., BROWN, J.D., HILL, K., HUGHES, J.P., SKAPER, S.D., AND MCNULTY, S., TRPM2 channel opening in response to oxidative stress is dependent on activation of poly(ADP-riobose) polymerase. *Br J Pharmacol,* **2004**, Sep;143(1):186-92. doi: 10.1038/sj.bjp.0705914.

20. FONFRIA, E., MATTEI, C., HILL, K., BROWN, J.T., RANDALL, A., BENHAM, C.D., SKAPER, S.D., CAMPBELL, C.A., CROOK, B., MURDOCK, P.R., WILSON, J.M., MAURIO, F.P., OWEN, D.E., TILLING, P.L., AND MCNULTY, S., TRPM2 is elevated in the tMCAO stroke model, transcriptionally regulated, and functionally expressed in C13 microglia. *J Recept Signal Transduct Res,* **2006**, 26(3):179-98. doi: 10.1080/10799890600637522.

21. GAO, J., YU, H., SONG, Q., AND LI, X., Establishment of HEK293 cell line expressing green fluorescent protein-aquaporin-1 to determine osmotic water permeability. *Anal Biochem,* **2005**, Jul 1;342(1):53-8. doi: 10.1016/j.ab.2005.03.033.

22. HAPPEL, P., MOLLER, K., KUNZ, R., AND DIETZEL, I.D., A boundary delimitation algorithm to approximate cell soma volumes of bipolar cells from topographical data obtained by scanning probe microscopy. *BMC Bioinformatics,* **2010** Jun 15;11:323. doi: 10.1186/1471-2105-11-323.

23. HAYABUCHI, Y., The Action of Smooth Muscle Cell Potassium Channels in the Pathology of Pulmonary Arterial Hypertension. *Pediatr Cardiol,* **2017** Jan;38(1):1-14. doi: 10.1007/s00246-016-1491-7.

24. HE, Y., HARA, H., AND NUNEZ, G., Mechanism and Regulation of NLRP3 Inflammasome Activation. *TrendsBiochem Sci,* **2016** Dec;41(12):1012-1021. doi: 10.1016/j.tibs.2016.09.002.

25. HE, Y., ZENG, M.Y., YANG, D., MOTRO, B., AND NUNEZ, G., NEK7 is an essential mediator of NLRP3 activation downstream of potassium efflux. *Nature,* **2016** Feb 18;530(7590):354-7. doi: 10.1038/nature16959.

26. HECQUET, C.M., AHMMED, G.U., AND MALIK, A.B., TRPM2 channel regulates endothelial barrier function. *Adv Exp Med Biol,* **2010**;661:155-67. doi: 10.1007/978-1-60761-500-2_10.

27. HEINER, I., JORG, E., HALASZOVICH, C.R., WEHAGE, E., JUNGLING, E., ZITT, C., AND LUCKHOFF, A., Expression profile of the transient receptor potential (TRP) family in neutrophil granulocytes: evidence for currents through long TRP channel 2 induced by ADP-ribose and NAD. *Biochem J,* **2003** May 1;371(Pt3):1045-53. doi: 10.1042/BJ20021975.

28. HINES, D.J, HINES, R.M., MULLIGAN, S.J., AND MACVICAR, B.A., Microglia processes block the spread of damage in the brain and require functional chloride channels. *Glia,*

2009 Nov 15;57(15):1610-8., doi: 10.1002/glia.20874.

29. HOPPERTON, K.E, MOHAMMAD, D., TREPANIER, M.O., GIULIANO, V., AND BAZINET, R.P., Markers of microglia in post-mortem brain samples from patients with Alzheimer's disease: a systemic review. *Mol Psychiatry,* **2018** Feb;23(2):177-198., doi: 10.1038/mp.2017.246.

30. HUANG, Y., WINKLER, P.A., SUN, W., LÜ, W., AND DU, J., Architecture of the TRPM2 channel and its activation mechanism by ADP-ribose and calcium. *Nature,* **2018** Oct;562(7725):145-149., doi: 10.1038/s41586-018-0558-4.

31. HUANG, Y., ROTH, B., LÜ, W., AND DU, J., Ligand recognition and gating mechanism through three Ligand-binding sites of human TRPM2 channel. *Elife,* **2019** Sep 12;8:350175, doi: 10.7554/eLife.50175.

32. ISHII, M., SHIMIZU, S., HARA, Y., HAGIWARA, T., MIYAZAKI, A., MARI, Y., AND KIUCHI, Y., Intracellular-produced hydroxyl radical mediates H2O2-induced Ca2+ influx and cell death in rat beta-cell line RIN-5F. *Cell Calcium,* **2006** Jun;39(6):487-94. doi: 10.1016/j.ceca.2006.01.013.

33. ISLAM, M.S., Calcium Signaling: From Basic to Bedside. *Adv Exp Med,* **2020**;1131:1-6. doi: 10.1007/978-3-030-12457-1_1.

34. JEONG, H., KIM, Y.H., LEE, Y., JUNG, S.J., AND OH, S.B., TRPM2 contributes to LPC-induced intracellular Ca^{2+} influx and microglial activation. *Biochem Biophys Res Commun,* **2017** Apr 1;485(2):301-306. doi: 10.1016/j.bbrc.2017.02.087.

35. JURGA, A.M., PALECZNA, M., AND KUTER, K., Overview of General and Discriminating Markers of Differential Microglia Phenotypes. *Front Cell Neurosci,* **2020** Aug 6;14:198. doi: 10.3389/fncel.2020.00198.

36. KACIK, M., OLIVAN-VIGUERA, A., AND KOHLER, R., Modulation of K(Ca)3.1 channels by eicosanoids, omega-3 fatty, and molecular determinants. *PLoS One,* **2014** Nov 5;9(11):e112081., doi: 10.1371/journal.pone.0112081.

37. KANEKO, Y., AND SZALLASI, A., Transient receptor potential (TRP) channels: a clinical perspective. *Br J Pharmacol,* **2014** May;171(10):2474-507., doi: 10.1111/bph.12414.

38. KASHIO, M., SOKABE, T., SHINTAKU, K., UEMATSU, T., FUKUTA, N., KOBAYASHI, N., MORI, Y., AND TOMINAGA, M., Redix-signal mediated sensitization of transient receptor potential melastatin 2 (TRPM2) to temperature affects macrophage functions. *Proc Natl Acad Sci USAl,* **2012** Apr 24;109(17):6745-50. doi: 10.1073/pnas.1114193109.

39. KETTENMANN, H., HANISCH, U.K., NODA, M., AND VERKHRATSKY, A., Physiology of microglia. *Physiol Rev,* **2011** Apr;91(2):461-553. doi: 10.1152/physrev.00011.2010.

40. KING, B., RIZWAN, A.P., ASMARA, H., HEATH, N.C., ENGBERS, J.D.T., DYKSTRA, S., BARTOLETTI, T.M., HAMEED, S., ZAMPONI, G.W., AND TURNER, R.W., IKCa channels are a critical determinant of the slow AHP in CA1 pyramidal neurons. *Cell Rep,* **2015** Apr 14;11(2):175-82. doi: 10.1016/j.celrep.2015.03.026.

41. KOLESNIKOV, D., PEREVOZNIKOVA, A., GUSEV, K., GLUSHANKOVA, L., KAZNACHEYEVA, E., AND SHALYGIN, A., Electrophysiological Properties of Endogenous Single Ca^{2+} Activated Cl^{-} Channels Induced ny Local Ca^{2+} Entry en HEK293. *Int J Mol Sci,* **2021** Apr 30;22(9):4767., doi: 10.3390/ijms22094767.

42. KOLISEK, M., BECK, A., FLEIG, A., AND PENNER, R., Cyclic ADP-ribose and hydrogen peroxide synergize with ADP-ribose in the activation of TRPM2 channels. *Mol Cell,* **2005** Apr1; 18(1):61-9., doi: 10.1016/j.molcel.2005.02.033.

43. KRAFT, R., GRIMM, C., GROSSE, K., HOFFMANN, A., SAUERBRUCH, S., KETTENMANN, H., SCHULTZ, G., AND HARTENECK, C., Hydrogen peroxide and ADP-ribose induce TRPM2-mediated calcium influx and cation currents in microglia. *Am J Physiol Cell Physiol,* **2004** Jan;286(1):C129-37., doi: 10.1152/ajpcell.00331.2003.

44. KRAFT, R., STIM and ORAI proteins in the nervous system. *Channels (Asutin),* **2015** 2015 ;9(5):245-52., doi: 10.1080/19336950.2015.1071747.

45. KSHATRI, A.S., GONZALEZ-HERNANDEZ, A., AND GIRALDEZ, T., Physiological Roles and Therapeutic Potential of Ca^{2+} Activated potassium Channels in the Nervous System. *Front Mol Neurosci,* **2018** Jul 30;11:258, doi: 10.3389/fnmol.2018.00258.

46. LALLET-DAHER, H., ROUDBARAKI, M., BAVENCOFFE, A., MARIOT, P., GACKIERE, F., BIDAUX, G., URBAIN, R., GROSSET, P., DECOURT, P., FLEURISSE, L., SLOMIANNY, C., DEWAILLY, E., MAUROY, B., BONNAL, J.L., SKRYMA, R., AND PREVARSKAYA, N., Intermediate-conductance Ca^{2+} -activated K^{+} channels (IK_{Ca1}) regulate human prostate cancer

cell proliferation through a close control of calcium entry. *Oncogene,* **2009** Apr 16;28(15):1792-806. doi: 10.1038/onc.2009.25 Epub 2009 Mar 9.

47. LEDOUX, J., WERNER, M.E., BRAYDEN, J.E., AND NELSON, M.T., Calcium-activated potassium channels and the regulation of vascular tone. *Physiology (Bethesda),* **2006** Feb;21:69-78., doi: 10.1152/physiol.00040.2005.

48. LEE, M., CHO, T., JANTARATNOTAI, N., WANG, Y.T., MCGEER, E., AND MCGEER, P.L., Depletion of GSH in glial cells induces neurotoxicity: relevance to aging and degenerative neurological diseases. *FASEB J,* **2010** Jul;24(7):2533-45., doi: 10.1096/fj.09-149997.

49. LENG, F., AND EDISON, P., Neuroinflammation and microglia activation in Alzheimer disease: where do we go from here. *Nat Rev Neurol,* **2021** Mar; 17(3):157-172., doi: 10.1038/s41582-020-00435-y.

50. LONGDEN, T.A., DUNN, K.M., DRAHEIM, H.J., NELSON, M.T., WESTON, A.H., AND EDWARDS, G., Intermediate-conductance calcium-activated potassium channels participate in neurovascular coupling. *Br J Pharmacol,* **2011** Oct;164(3):922-33., doi: 10.1111/j.1476-5381.2011.01447.x.

51. LUO, X., LI, M., ZHAN, K., YANG, W., ZHANG, L., WANG, K., YU, P., AND ZHANG, L., Selective inhibition of TRPM2 channel by two novel synthesized ADPR analogues. *Chem Biol Drug Des,* **2018** Feb; 91(2):552-556., doi: 10.1111/cbdd.13119.

52. MAEZAWA, I., JENKINS, D.P., JIN, B.E., AND WULFF, H., Microglia KCa3.1 Channels as a Potential Therapeutic Target for Alzheimer's Disease. *Int J Alzheimers Dis,* **2012;**2012:868972. doi: 10.1155/2012/869872.

53. MARIN-TEVA, J.L., CUADROS, M.A., MARTIN-OLIVA, D., AND NAVASCUES, J., Microglia and neuronal cell death. *Neuron Glia Biol,* **2011** Feb;7(1):25-40. doi: 10.10117/S1740925X12000014.

54. MUNARON, L., ANTONIOTTI, S., AND LOVISOLO, D., Intracellular calcium signals and control of cell proliferation: how many mechanisms?. *J Cell Mol Med,* **2004** Apr; 8(2): 161-168., doi: 10.1111/j.1582-4934.2004.tb00271.x.

55. MINCHEVA-TASHEVA, S., OBIS, E., TAMARIT, J., AND ROS, J., Apoptotic cell death and altered calcium homeostasis caused by frataxin depletion in dorsal root ganglia neurons can

be prevented bu BH4 domain of Bcl-xL protein. *Hum Mol Genet,* **2014** Apr 1;23(7):1829-41. doi: 10.1093/hmg/ddt576..

56. NGUYEN, H.M., GROSSINGER, E.M., HORIUCHI, M., DAVIS, K.W., JIN, L.W., MAEZAWA, I., AND WULFF, H., Differential Kv1.3, KCa3.1, and Kir2.1 expression in 'classically" and 'alternatively" activated microglia. *Glia,* **2017** Jan;65(1):106-121. doi: 10.1002/glia.23078. Epub 2016 Oct 3.

57. NILIUS, B., OWSIANIK, G., VOETS, T., AND PETERS, J.A., Transient receptor potential cation channels in disease. *Physiol Rev,* **2007** Jan; 87(1):165-217., doi: 10.1152/physrev.00021.2006.

58. NILIUS, B., AND OWSIANIK, G., The transient receptor potential family of ion channels. *Genome Biol,* **2011**; 12(3):218. doi: 10.1186/gb-2011-12-3-218.

59. NIMMERJAHN, A., KIRCHHOFF, F., AND HELMCHEN, F., Resting microglia cells are highly dynamic surveillants of brain parenchyma in vivo. *Science,* **2005** May 27;308(5726):1314-8. doi: 10.1126/science.1110647.

60. NISHIMOTO, R., DEROUICHE, S., ETO, K., DEVECI, A., KASHIO, M., KIMORI, Y., MATSUOKA, Y., MORIMATSU, H., NABEKURA, J., AND TOMINAGA, M., Thermosensitive TRPV4 channels mediate temperature-dependent microglia movement. *Proc Natl Acad Sci USA,* **2021** Apr 27;118(17):e2012894118. doi: 10.1073/pnas.2012894118.

61. OLAH, M.E., JACKSON, M.F., LI, H., PEREZ, Y., SUN, H.S., KIYONAKA S., MORI, Y., TYMIANSKI, M., AND MACDONALD, J.F., Ca2+-dependent induction of TRPM2 currents in hippocampal. *J Physiol,* **2009** Mar 1;587(Pt 5):965-79. doi: 10.1113/jphysiol.2008.162289.

62. PEDARZANI, P., AND STOCKER, M., Molecular and cellular basis of small—and intermediate-conductance, calcium-activated potassium channel function in the brain. *Cell Mol Life Sci,* **2008** Oct;65(20):3196-217. doi: 10.1007/s00018-008-8216-x.

63. PINTO, M.C.X., KIHARA, A.H., GOULART, V.A.M., TONELLI, F.M.P., GOMES, K.N., ULRICH, H., AND RESENDE, R.R., Calcium signaling and cell proliferation. *Cell Signal,* **2015** Nov ;27(11):2139-49. doi: 10.1016/j.cellsig.2015.08.006.

64. RAFFAELO, A., MAMMUCARI, C., GHERARDI, G., AND RIZZUTO, R., Calcium at the Center of Cell Signaling: Interplay between Endoplamic Reticulum, Mitochondria, and

Lysosomes. *Trends Biochem Sci,* **2016**; Dec;41(12):1035-1049. doi: 10.1016/j.tibs.2016.09.001.

65. RIZZUTO, R., AND POZZAN, T., Microdomains of intracellular Ca2+: molecular determinants and functional consequences. *Physiol Rev,* **2006** Jan;86(1):369-408. doi: 10.1152/physrev.00004.2005.

66. SARLUS, H., AND HENEKA, N.T., Microglia in Alzheimer's disease. *J Clin Invest,* **2017**; Sep 1;127(9):3240-3249., doi: 10.1172/JCI90606.

67. SCHNEIDER, S.W., PAGEL, P., ROTSCH, C., DANKER, T., OBERLEITHNER, H., RADMACHER, M., AND SCHWAB, A., Volume dynamics in migrating epithelial cells measured with atomic force microscopy. *Pflugers Arch,* **2000** Jan;439(3):1297-303. doi: 10.1007/s004249900176.

68. SCHWAB, A., FABIAN, A., HANLEY, P.J., AND STOCK, C., Role of ion channels and transporters in cell migration. *Physiol Rev,* **2012** Oct;92(4):1865-913. doi: 10.1152/physrev.00018.2011.

69. SFORNA, L., MEGARO, A., PESSIA, M., FRANCIOLONI, F., AND CATACUZZENO, L., Structure, Gating and Basic Function of the Ca^{2+}-activated K Channel of Intermediate Conductance. *Curr Neuropharmacol,* **2018**; 16(5):608-617., doi: 10.2174/1570159X15666170830122402.

70. SHEN, Y., LEE, Y.S., SOELAIMAN, S., BERGSON, P., LU, D., CHEN, A., BECKINGHAM, K., GRABAREK, Z., MRKSICH, M., AND TANG, W.J., Physiological calcium concentration regulate calmodulin binding and catalysis of adenylyl cyclase exotoxins. *EMBO J,* **2002** Dec 16;21(24):6721-32., doi: 10.1093/emboj/cdf681.

71. SITA, G., HRELIA, P., GRAZIOSI, A., RAVEGNINI, G., AND MORRONI, F., TRPM2 in the Brain: Role in Health and Disease. *Cells,* **2018** Jul 22;7(7):82. doi: 10.3390/cells7070082.

72. SKAPER, S.D., FACCI, L., AND GIUSTI, P., Intracellular ion channel CLIC1: involvement in microglia-mediated β-amyloid peptide (1-42) neurotoxicity. *Neurochem Res,* **2013** Sep;38(9):1801-8., doi: 10.1007/s11064-013-1084-2.

73. SOLDANI, C., AND SCOVASSI, A.I., Poly(ADP-ribose) polymerase-1 cleavage during apoptosis: an update. *Apoptosis,* **2002** Aug;7(4):321-8., doi: 10.1023/a:1016119328968.

74. STARKUS, J., BECK, A., FLEIG, A., AND PENNER, R., Regulation of TRPM2 by Extra- and Intracellular Calcium. *J Gen Physiol,* **2007** Oct;130(4):427-40., doi: 10.1085/jgp.200709836.

75. SUMOZA-TOLEDO, A., LANGE, I., CORTADO, H., BHAGAT, H., MORI, Y., FLEIG, A., PENNER, R., AND PARTIDA-SANCHEZ, S., Dendritic cell maturation and chemotaxis is regulated by TRPM2-mediated lysosomal Ca2+ release. *FASEB J,* **2011** Oct;25(10):3539-42. doi: 10.1096/fj.10-178483.

76. SUN, Z., GONG, W., ZHANG, Y., AND JIA, Z., Physiological and Pathological Roles of Mammalian NEK7. *Front Physiol,* **2020** Dec 7;11:606996., doi: 10.3389/fphys.2020.606996.

77. SUPPIRAMANIAM, V., ABDEL-RAHMAN, E.A., BUABEID, M.A., AND PARAMESHWARAN, K., 10.09 Ion Channels. *Comprehensive Toxicology (second Edition),* **2010** doi: 10.1016/B978-0-08-046884-6.01310-5.

58. SZASZI, K., SIROKMANY, G., DI CIANO-OLIVEIRA, C., ROTSTEIN, O.D., AND KAPUS, A., Depolarisation induces Rho-Rho kinase-mediated myosin light chain phosphorylation in kidney tubular cells. *Am J Physiol Cell Physiol,* **2004** Sep;289(3):C673-85 doi: 10.1152/ajpcell.00481.2004.

78. SZOLLOSI, A., Two Decades of Evolution of Our Understanding of the Transient Receptor Potential Melastin 2 (TRPM2) Cation Channel. *Life,* **2021** Apr 27;11(5):397., doi: 10.3390/life11050397.

79. TAO, Y., YAN, D., YANG, Q., ZENG, R., AND WANG, Y., Low K^+ Promotes NF-κB/DNA Binding in Neuronal Apoptosis Induced by K^+ Loss. *Mol Cell Biol,* **2006** Feb,26(3):1038-50., doi: 10.1128/MCB.26.3.1038-1050.2006.

80. TAKAHASHI, N., KOZAI, D., KOBAYASHI, R., EBERT, M., AND MORI, Y., Role of TRPM2 in oxidative stress. *Cell Calcium,* **2011** Sep;50(3):279-87. doi: 10.1016/j.ceca.2011.04.006.

81. TAKAYAMA, Y., SHIBASAKI, K., SUZUKI, Y., YAMANAKA, A., AND TOMINAGA, M., Modulation of water efflux through functional interaction between TRPV4 and TMEM16A/anoctamin 1. *FASEB J,* **2014** May;28(5):2238-48. doi: 10.1096/fj.13-243436. Epub 2014 Feb 7.

82. THEI, L., IMM, J., KAISIS, E., DALLAS, M.L., AND KERRIGAN, T.L., Microglia in

Alzheimer's Disease: A Role for Ion Channels. *Front Neurosci,* **2018** Sep;28;12:676. doi: 10.3389/fnins.2018.00676.

83. TOGASHI, K., HARA, Y., TOMINAGA, T., HIGASHI, T., KONISHI, Y., MORI, Y., AND TOMINAGA, M., TRPM2 activation by cyclic ADP-ribose at body temperature is involved in insulin secretion. *EMBO J,* **2006** May 3;25(9):1804-15. doi: 10.1038/sj.emboj.7601083.

84. TOMBETTA-LIMA, M., KRABBENDAM, I.E., AND DOLGA, A.M., Calcium activated potassium channels: implication for aging and age-related neurodegeneration. *Int J Biochem Cell Biol,* **2020** Jun; 123:105748. doi: 10.1016/j.biocel.2020.105748.

85. TONG, Q., ZHANG, W., CONRAD, K., MOSTOLLER, K., CHEUNG, J.Y., PETERSON, B.Z., AND MILLER, B.A., Regulation of the transient receptor potential channel TRPM2 by the Ca2+ sensor calmodulin. *J Biol Chem,* **2006** Apr 7;281(14):9076-85. doi: 10.1074/jbc.M510422200.

86. TOYAMA, K., WULFF, H., CHANDY, K.G., AZAM, P., RAMAN, G., SAITO, T., FUJIWARA, Y., MATTSON, D.L., DAS, S., MELVIN, J.E., PRATT, P.F., HATOUM, O.A., GUTTERMAN, D.D., HARDER, D.R., AND MIURA, H., The intermediate-conductance calcium-activated potassium channel KCa3.1 contributes to atherogenesis in mice and humans. *J Clin Invest,* **2008** Sep;118(9):3025-37. doi: 10.1172/JCI30836.

87. TURLOVA, E., FENG, Z.P., AND SUN, H.S., The role of TRPM2 channels in neurons, glial cells and the blood-brain barrier in cerebral ischemia and hypoxia. *Acta Pharmacol Sin,* **2018** May; 39(5):713-721. doi: 10.1038/aps.2017.194.

88. WAHEED, F., SPEIGHT, P., KAWAI, G., DAN, Q., KAPUS, A., AND SZASZI, K., Extracellular signal-regulated kinase and GEF-H1 mediate depolarization-induced Rho activation and paracellular permeability increase. *Am J Physiol Cell Physiol,* **2010** Jun; 298(6)C:1376-87. doi: 10.1152/ajpcell.00408.2009.

89. WATKINS, S., AND SONTHEIMER, H., Hydrodynamic cellular volume changes enable glioma cell invasion. *J Neurosci,* **2011** Nov 23;31(47):17250-9. doi: 10.1523/JNEUROSCI.3938-11.2011.

90. WEISBROD, D., Small and Intermediate Calcium Activated Potassium Channels in the Heart: Role and Strategies in the Treatment of Cardiovascular Diseases. *Front Physiol,* **2020** Nov 23;11:590534. doi: 10.3389/fphys.2020.590534.

91. WOLF, S.A., BODDEKE, H.W.G.M., AND KETTENMANN, H., Microglia in Physiology and disease. *Annu Rev Physiol,* **2017** Feb 10;79:619-643. doi: 10.1146/annurev-physiol-022516-034406.

92. WULFF, H., AND CASTLE, N.A., Therapeutic potential of KCa3.1 blockers: recent advances and promising trends. *Expert Rev Clin Pharmacol,* **2010** May;3(3):385-96. doi: 10.1586/ecp.10.11.

93. XIE, Y.F., BELROSE, J.C., LEI, G., TYMIANSKI, M., MORI, Y., MACDONALD, J.F., AND JACKSON, M.F., Dependence of NMDA/GSK-3β mediated metaplasticity on TRPM2 channels at hippocampal CA3-CA1 synapses. *Mol Brain,* **2011** Dec 21;4:44. doi: 10.1186/1756-6606-4-44.

94. YANG, Z., KIRTON, H.M., MACDOUGALL, D.A., BOYLE, J.P., DEUCHARS, J., FRATER, B., PONNAMBALAM, S., HARDY, M.E., WHITE, E., CALAGHN, S.C., PEERS, C., AND STEELE, D.S., The Golgi apparatus is a functionally distinct Ca2+ store regulated by the PKA and Epac branches of the β1-adrenergic signaling pathway. *Sci Signal,* **2015** Oct 13;8(398):ra101. doi: 10.1126/scisignal.aaa7677.

95. YILDIZHAN, K., AND NAZIROGLU, M., Glutathione depletion and Parkinsonian neurotoxin MPP^+-induced TRPM2 channel activation play central roles in oxidative cytotoxicity and inflammation in microglia. *Mol Neurobiol,* **2020** Aug;57(8):3508-3525. doi: 10.1007/s12035-020-01974-7.

96. YU, S.P., AND KERCHNER, G.A., Endogenous voltage-gated potassium channels in human embryonic kidney (HEK293) cells. *J Neurosci Res,* **1998** Jun 1;52(5):612-7. doi: 10.1002/(SICI)1097-4547(19980601)52:5<612::AID-JNR13>3.0.CO;2-3.

97. ZHAO, Q., LI, J., KO, W.H., KWAN, Y.W., JIANG, L., SUN, L., AND YAO, X., TRPM2 promotes autophagic degradation in vascular smooth muscle. *Sci REP,* **2020** Nov 26;10(1):20719. doi: 10.1038/s41598-020-77620-y.